Interfacial Friction: From Roughness Effects to Rupture Front Propagation

Demirkan Çöker

Department of Aerospace Engineering
RUZGEM Center for Wind Energy
Middle East Technical University, Ankara, Türkiye

Research Scope

Physics and mechanics of fracture-friction-fatigue along interfaces in heterogeneous structures.

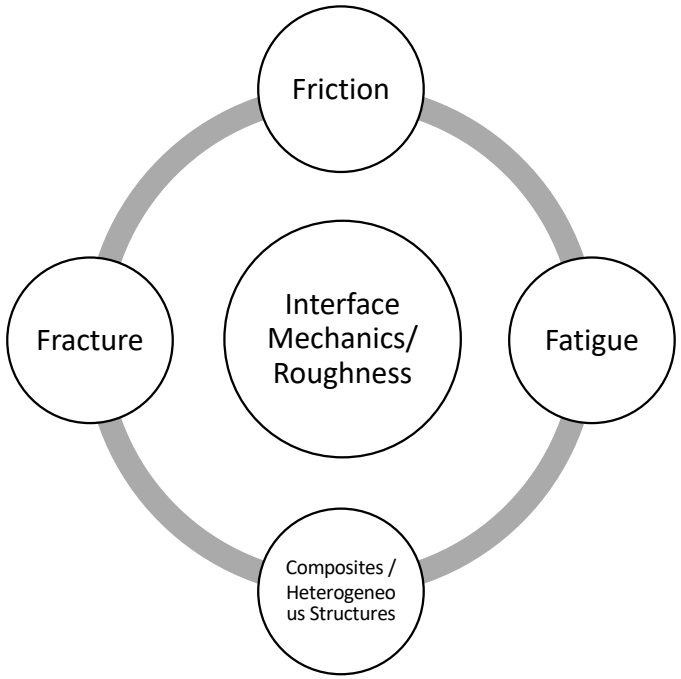

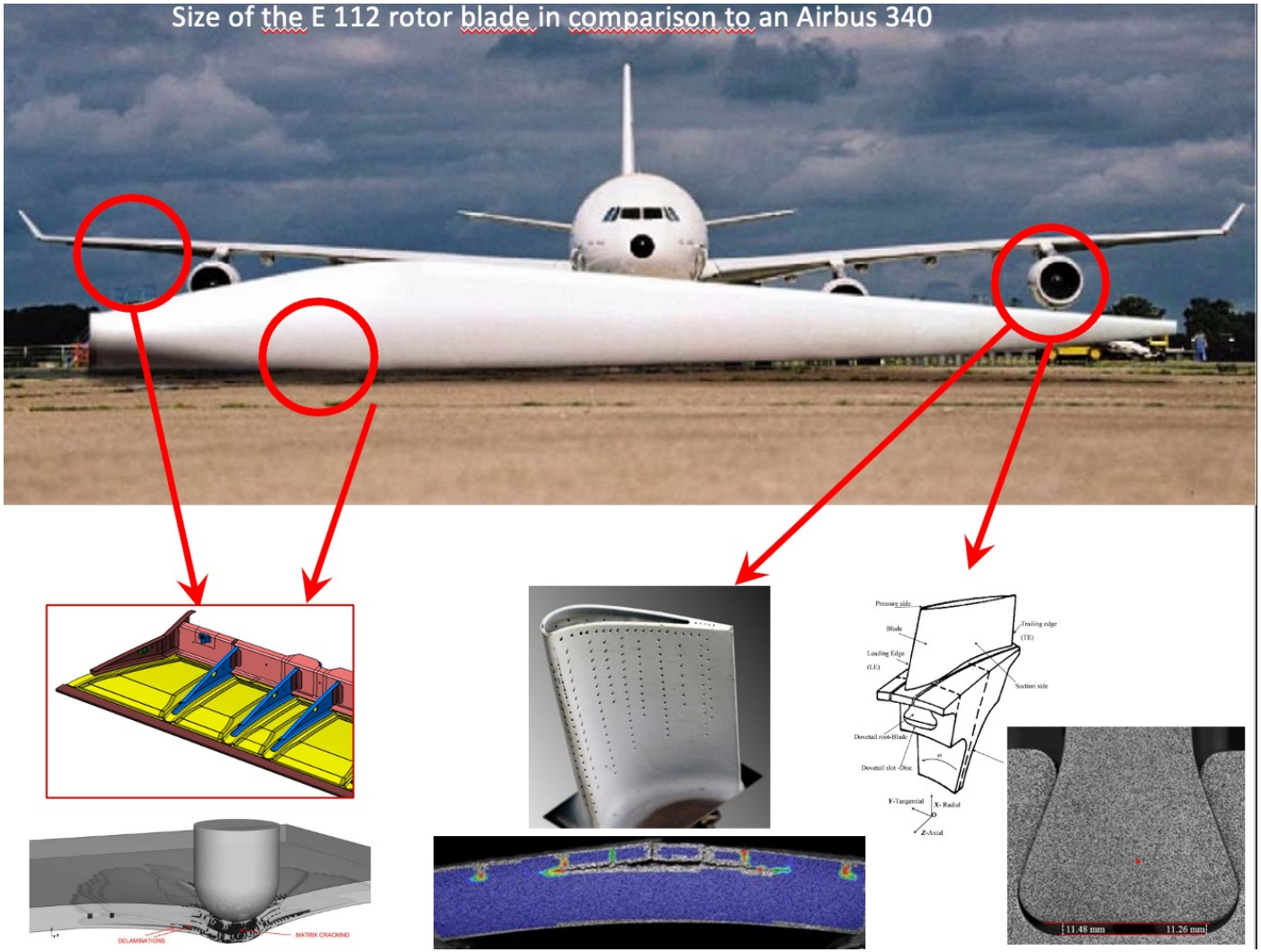

INTRODUCTION

Earthquakes, Friction, and Sliding Instability

Scope of Lecture

PART 1. Surface Roughness: Conditions for stick-slip vs steady sliding

PART 2. During the slip phase of the stick-slip behavior dynamic frictional sliding and rate- and state friction models

Earthquake Source Mechanics: Stick–Slip

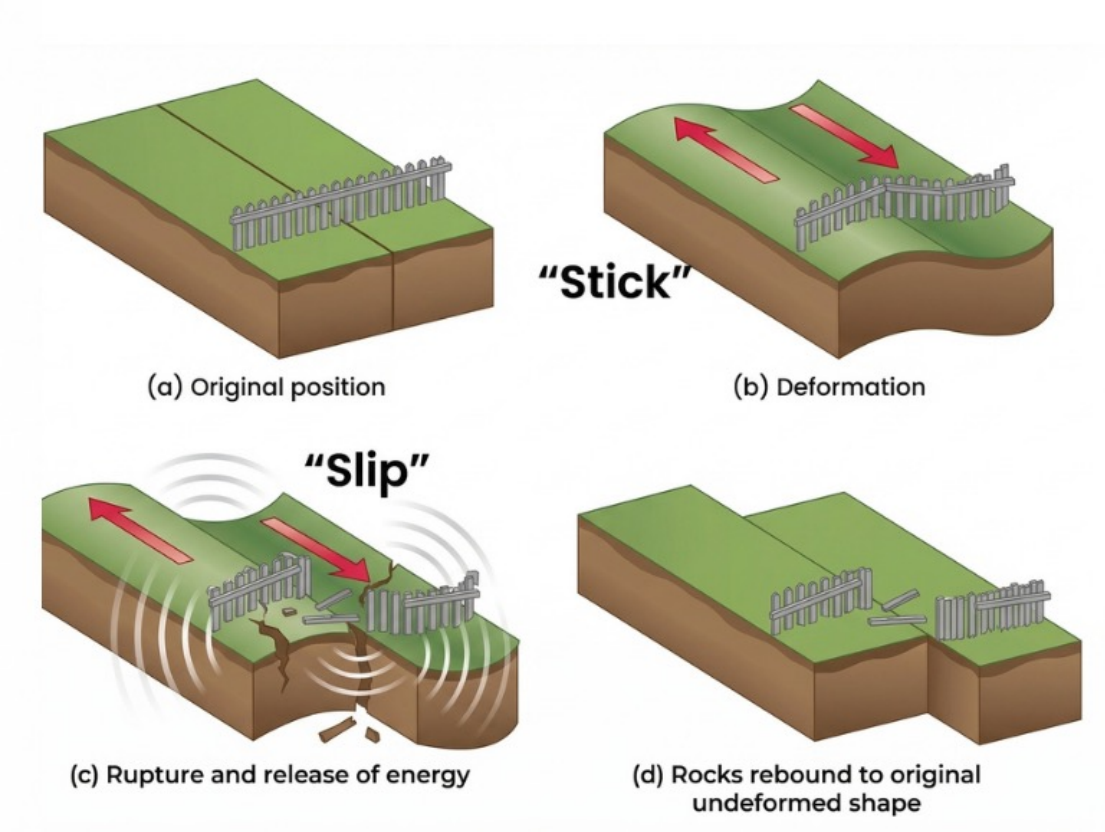

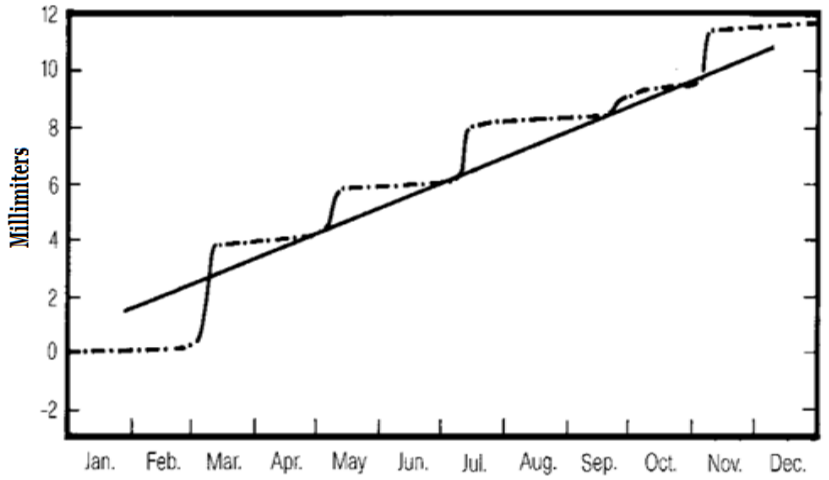

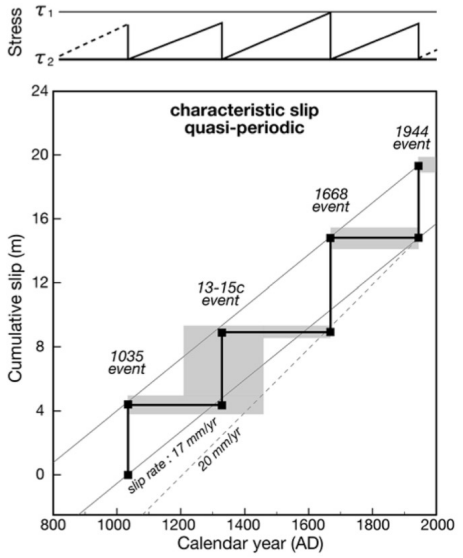

Fig. 5.22. Time-slip diagram for the Demir Tepe site in the Gerede segment. Shading indicates uncertainty in slip and dates. (From Kondo et al., 2010.)

(Scholz ,2002)

Fiber Pull-Out Experiments

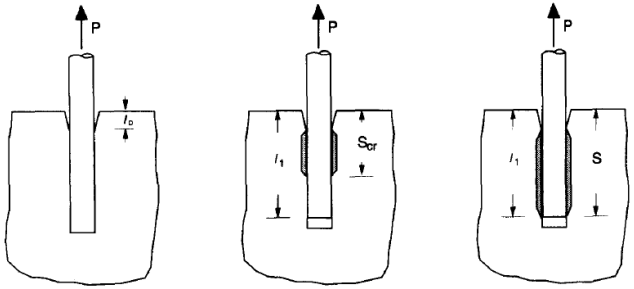

(i) Precursor of fiber pull-out: Semi-brittle debonding.

(ii) Fiber pull-out with limited active sliding zone. ($S_{cr} < l_1$)

(iii) Fiber pull-out with full active sliding zone. ($S_{cr} > l_1$)

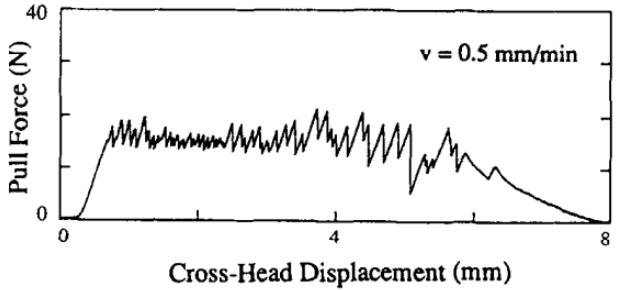

Tsai & Kim (*JMPS*, 1996)

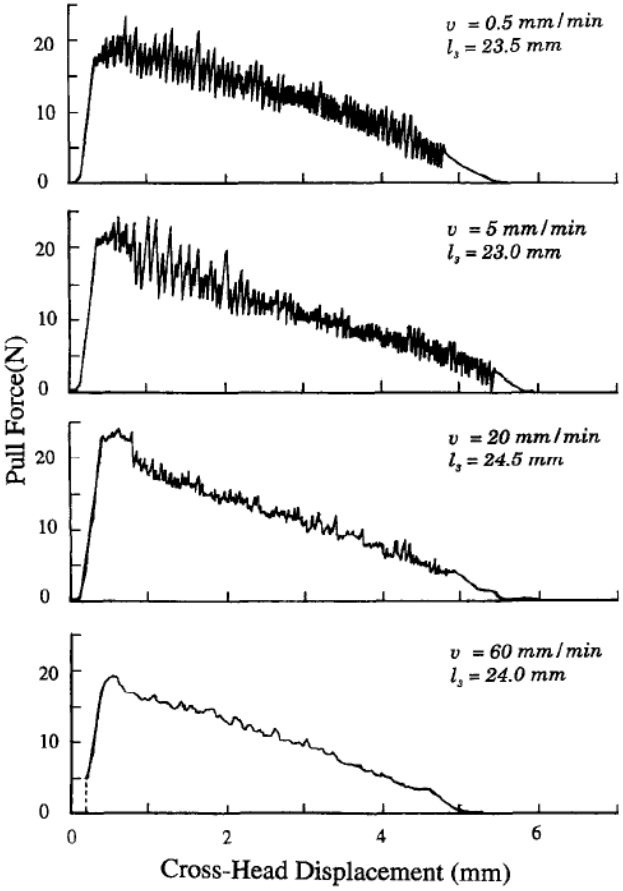

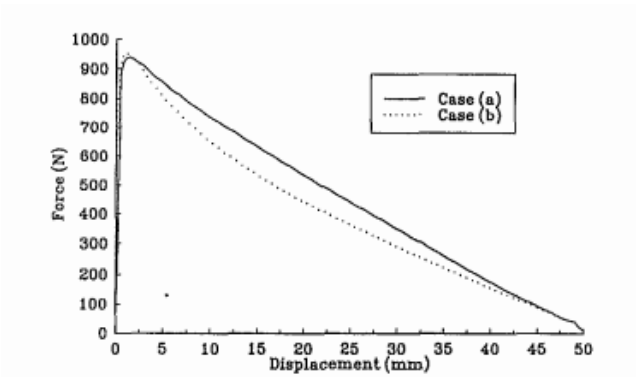

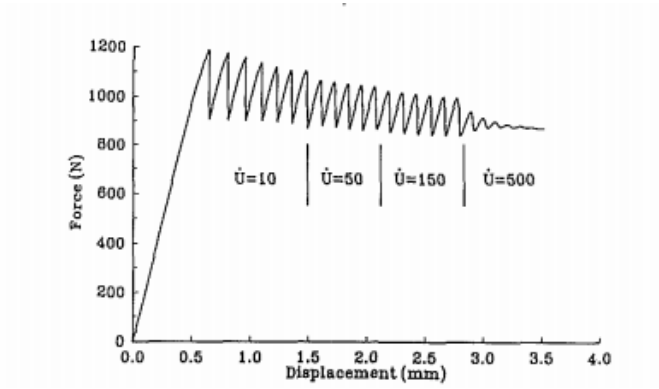

Povirk & Needleman (*JEMT*, 1993)

What affects the transition from stick-slip to steady-sliding behavior during frictional sliding?

- Roughness
- Initial compressive loading (normal load)
- Shear loading rate / velocity
- Stiffness
- Loading Geometry

Normal Load

Normal stress (σ_n): governs the magnitude of stress drops and the intensity of stick–slip instability

Higher σ_n → larger real contact area → stronger asperity interlocking → larger stress drops

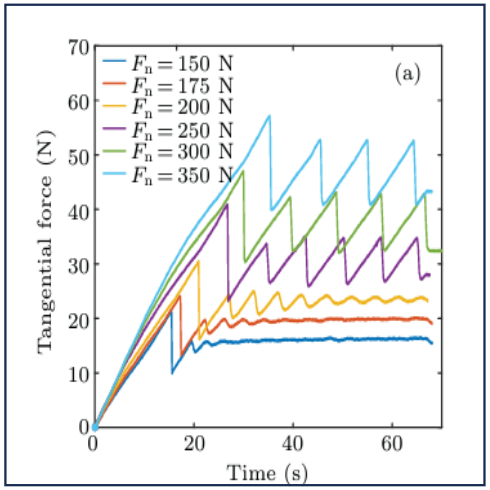

Han, Ding, Wu, and Yan (*Chinese Physical B*, 2022)

Shear Loading Rate

Loading (slip) rate: controls recurrence interval of stick–slip events via a power-law relation

Higher rates → shorter recurrence time → reduced time for interfacial strengthening → tendency toward stable sliding

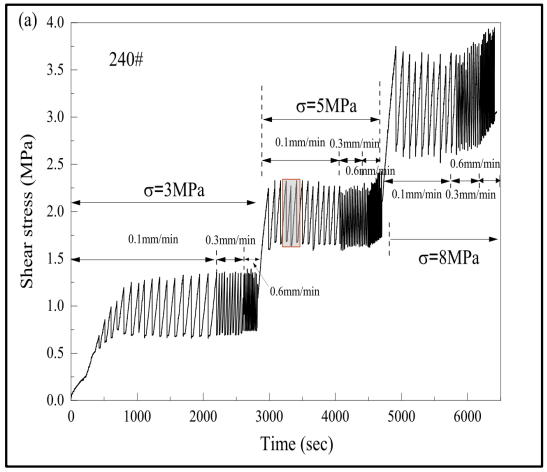

Zhou, He, Shou (*Tectonophysics*, 2021)

System Stiffness

Ratio of loading system stiffness to fault/interface stiffness determines whether stored elastic energy can be released suddenly

- Low system stiffness relative to interface weakening rate promotes stick–slip (classical instability criterion)
- Ohnaka (1973): stick–slip emerges from the interplay between system stiffness and interfacial contact structure

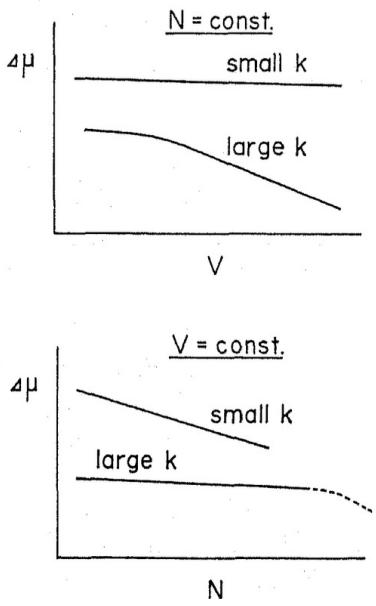

Ohnaka (1973)

Loading Geometry:

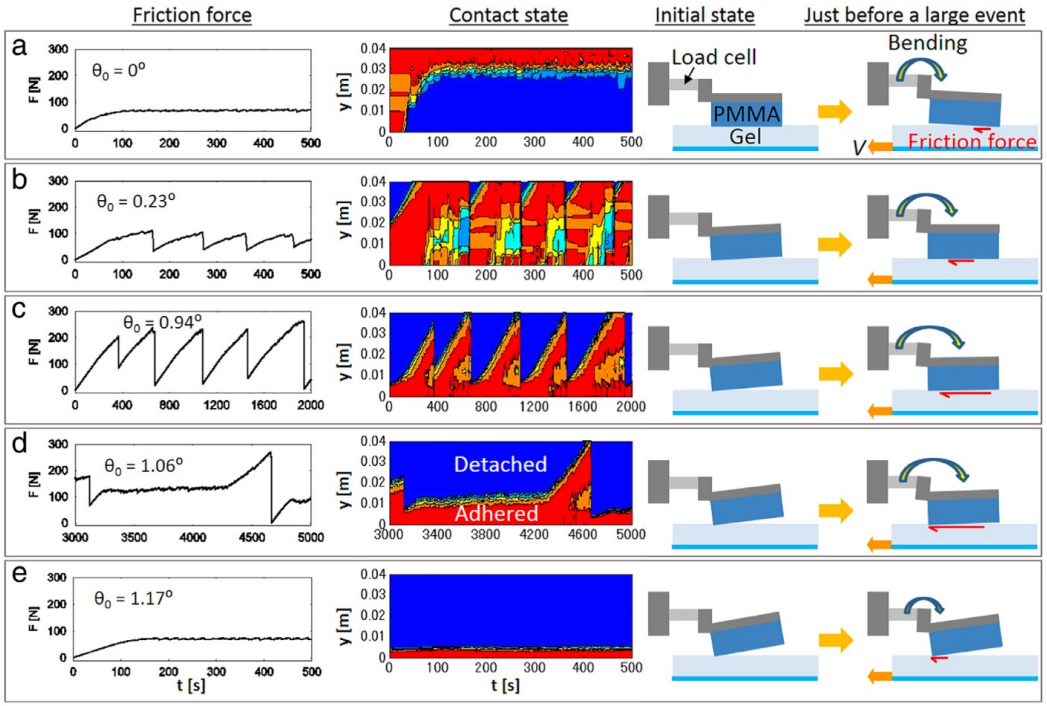

Fig. 2. Time variations of the friction forces $F(t)$ (left), the spatio-temporal maps of the contact state $C(y, t)$ (middle), and corresponding schematic pictures for the initial state and the state just before a large slip event (right). The initial inclination angle is (a) $\theta_0 = 0°$, (b) 0.23°, (c) 0.94°, (d) 1.06° and (e) 1.17°. The applied normal load F_N is 10 N in these experiments.

Yamaguchi, Sawae and Rubinstein (*Extreme Mech. Lett.*, 2016)

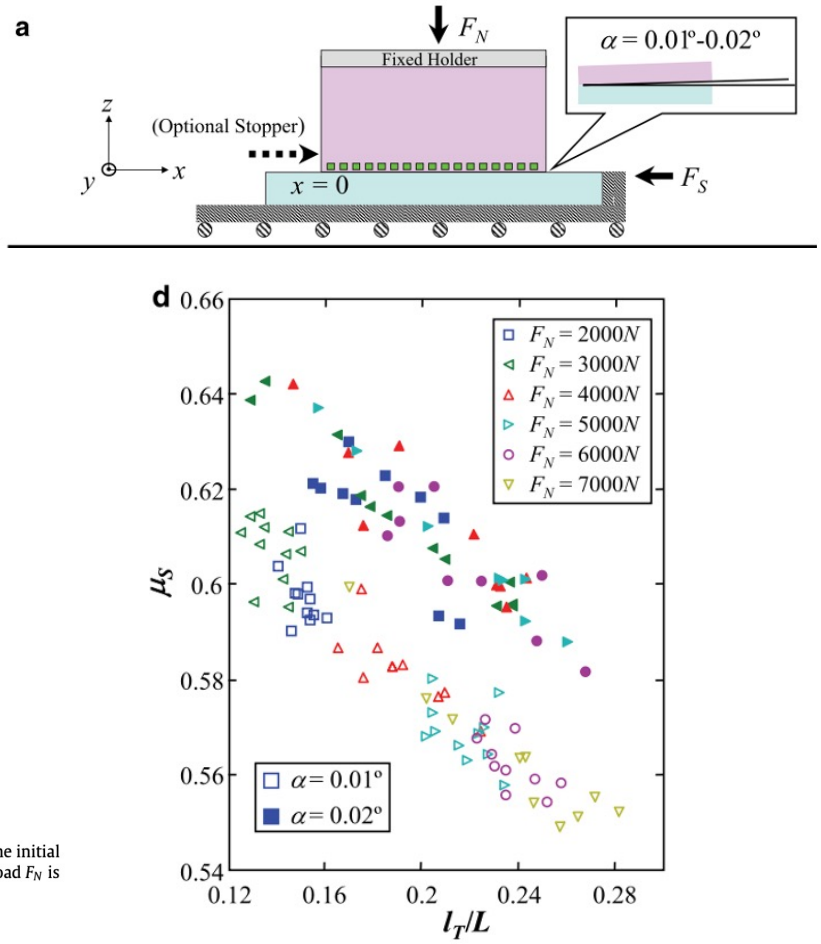

Ben-David & Fineberg (*Phys. Rev. Lett.*, 2011)

PART 1

Surface Roughness : *stable sliding to stick–slip*

Real Contact Area

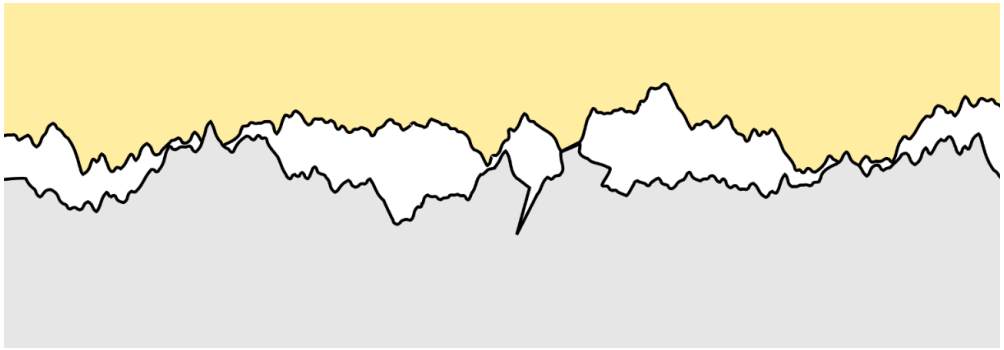

- Real contact area (A_r) is typically much smaller than the apparent (nominal) area (A_a), even for carefully prepared surfaces (Bowden & Tabor, 1950)
- Contact occurs at discrete spots — a population of microscopic asperity junctions — not over the full apparent area
- Greenwood–Williamson (1966): A_r scales approximately linearly with normal load for elastic-plastic contacts: $A_r \sim N/H$
- Friction force arises from the shear strength of these real contact junctions, not from an area-independent 'friction coefficient'

Stress Heterogeneity at the Interface

Real interfaces carry load through discrete asperity contacts, creating highly non-uniform stress fields.

This heterogeneity controls:

(1) where slip nucleates,

(2) how it propagates, and

(3) whether it becomes macroscopic.

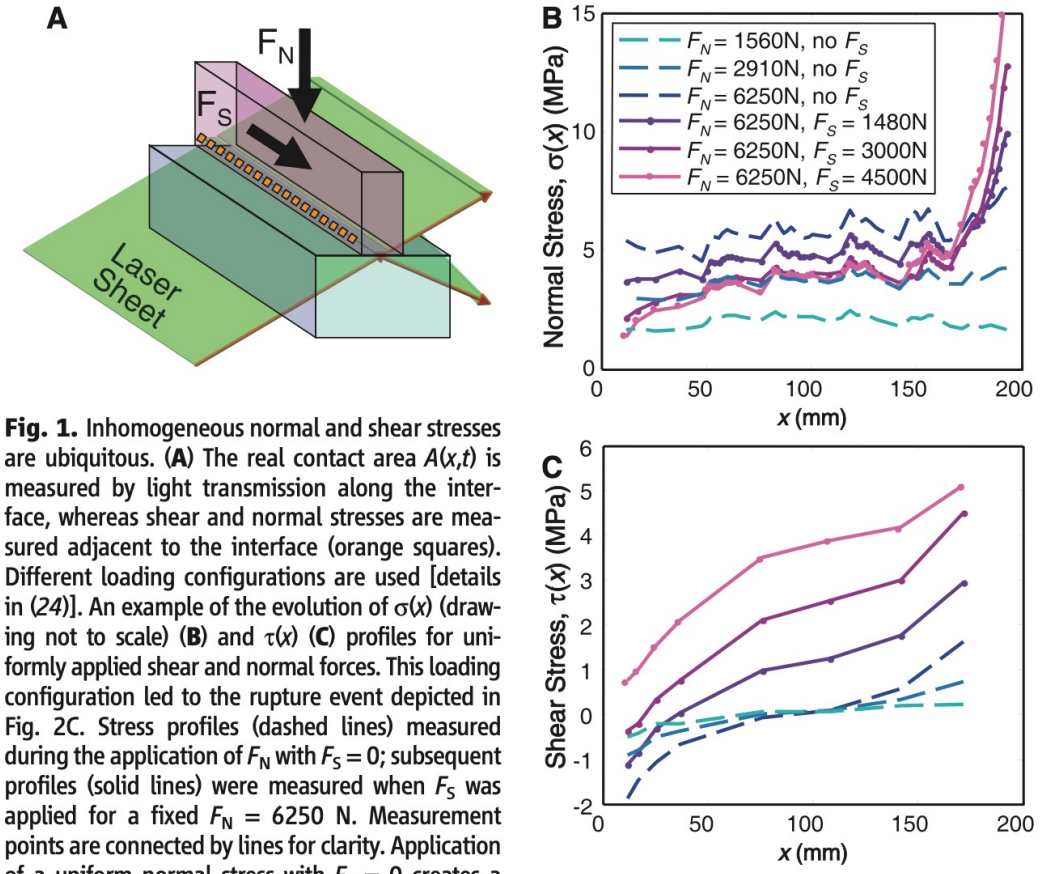

Fig. 1. Inhomogeneous normal and shear stresses are ubiquitous. (**A**) The real contact area $A(x,t)$ is measured by light transmission along the interface, whereas shear and normal stresses are measured adjacent to the interface (orange squares). Different loading configurations are used [details in (*24*)]. An example of the evolution of $\sigma(x)$ (drawing not to scale) (**B**) and $\tau(x)$ (**C**) profiles for uniformly applied shear and normal forces. This loading configuration led to the rupture event depicted in Fig. 2C. Stress profiles (dashed lines) measured during the application of F_N with $F_S = 0$; subsequent profiles (solid lines) were measured when F_S was applied for a fixed F_N = 6250 N. Measurement points are connected by lines for clarity. Application of a uniform normal stress with F_S = 0 creates a nonuniform antisymmetric $\tau(x)$ profile, solely as a result of differential Poisson expansion frustrated at the interface. Application of F_S increases the mean level of $\tau(x)$ while producing strong nonuniformity of $\sigma(x)$ near the block edges to compensate for external torque.

Ben-David , Cohen and Fineberg (*Science* 2010)

Roughness and Sliding Instability: Experimental Observations

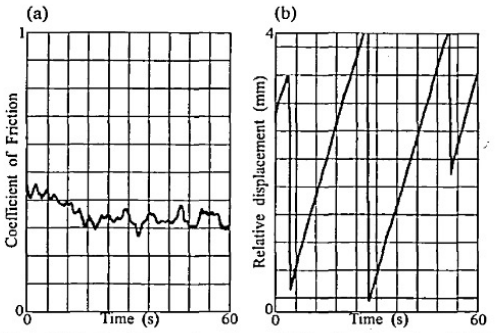

Fig. 3. Data record for rough surfaces (RMS value 49 μm) at 10 MPa normal pressure and 10 mm min^{-1} slip rate. The three large displacements in (b) correspond to repositioning of the laser transducers.

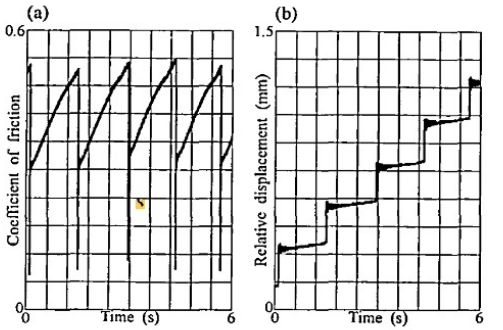

Fig. 4. Data record for intermediate surface roughness (RMS value 24 μm) at 10 MPa normal pressure and 10 mm min^{-1} slip rate.

Boissou, Petit and Barquins (*Wear*, 1998)

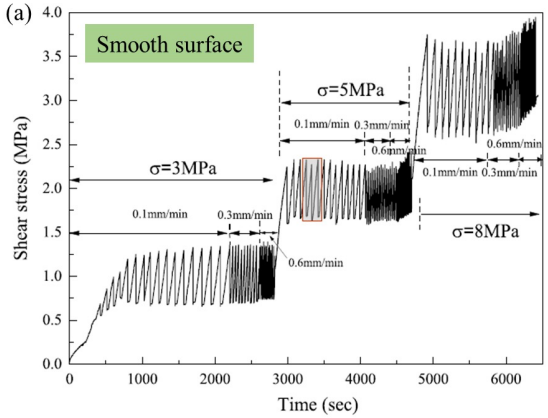

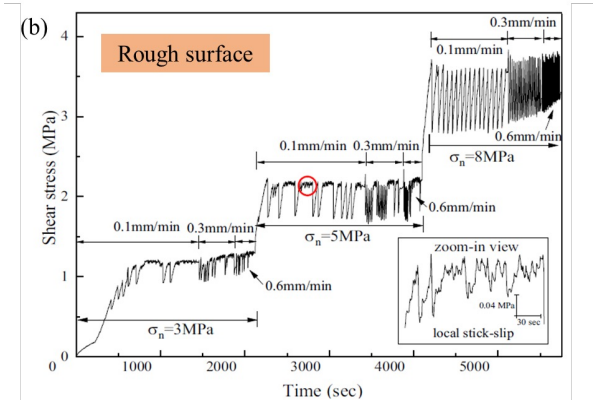

Zhou, He, Shou (*Tectonophysics*, 2021)

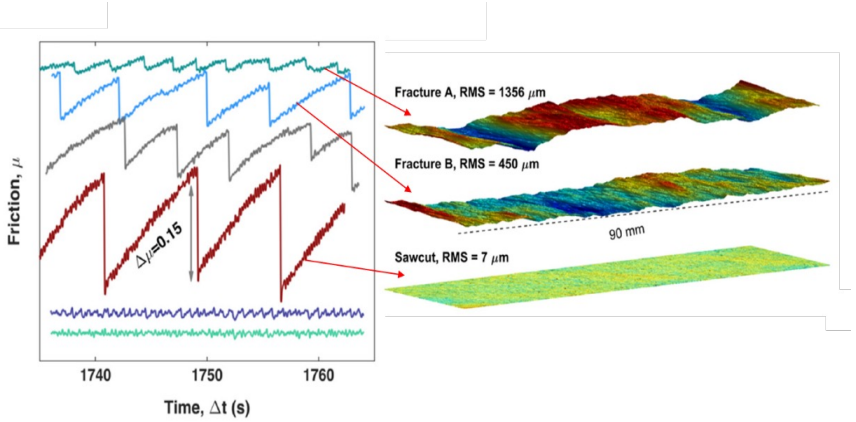

Morad D., Sagy A., Tal Y., and Hatzor Y. H. (*Earth and Planetary Science Letters*, 2022)

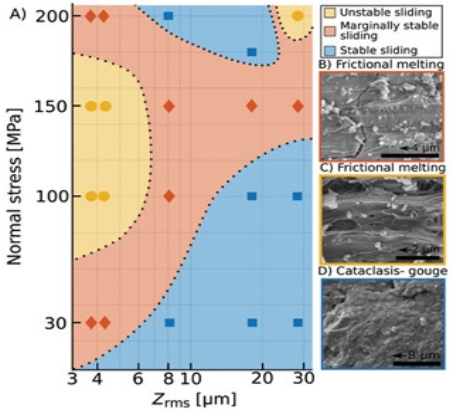

Harbord, Nielsen, Paola, and Holdsworth (*Geology*, 2017)

Experimental Observations using Photoelasticity and DIC

Effect of interface on the stress distribution

Photoelasticity reveals the full-field stress distribution near frictional interfaces in transparent materials (PMMA)

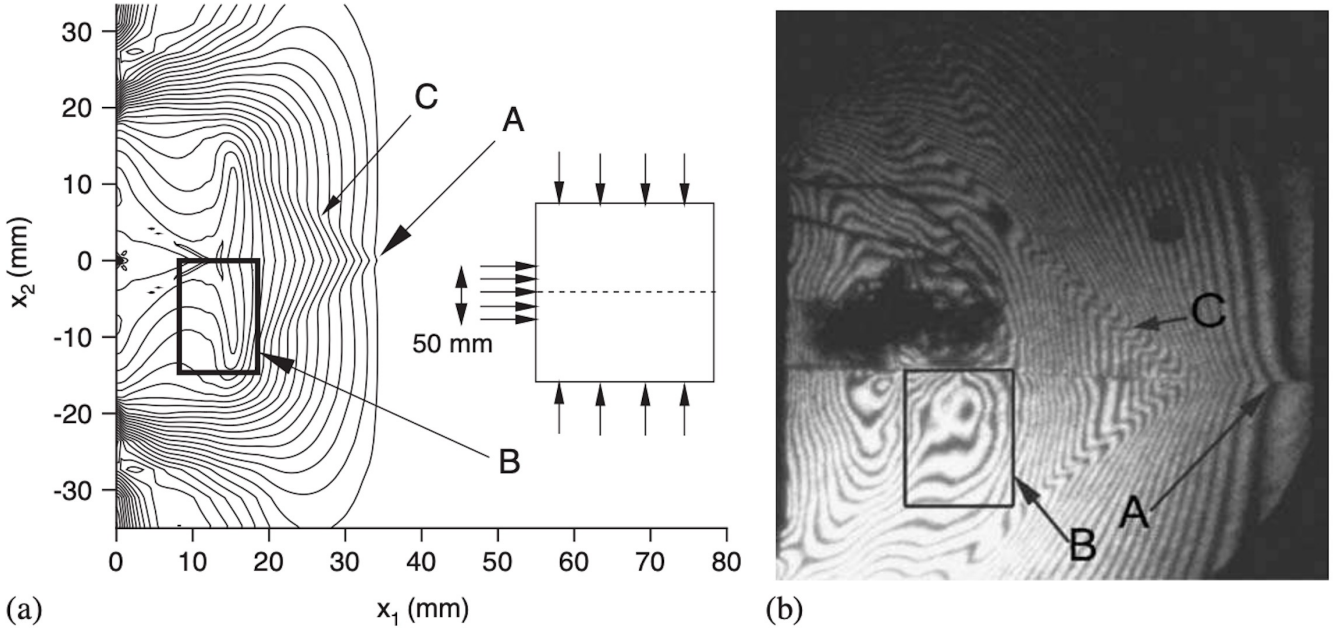

Fig. 7. Isochromatic fringe patterns due to loading symmetric with respect to the interface. (a) Computed isochromatic fringe patterns (contours of $\sigma_1 - \sigma_2$) at $t = 16\,\mu s$ for $\Sigma_0 = 10\,MPa$, $V_{imp} = 5\,m/s$, with the configuration analyzed shown in the inset. (b) Experimental isochromatic fringe patterns for $\Sigma_0 = 0\,MPa$, $V_{imp} = 58\,m/s$. In (b) the field of view is 130 mm in diameter.

Coker, Lykotrafitis, Rosakis, Needleman (*JMPS*, 2005)

Photoelasticity Observations of Interface Effects under Normal Loading

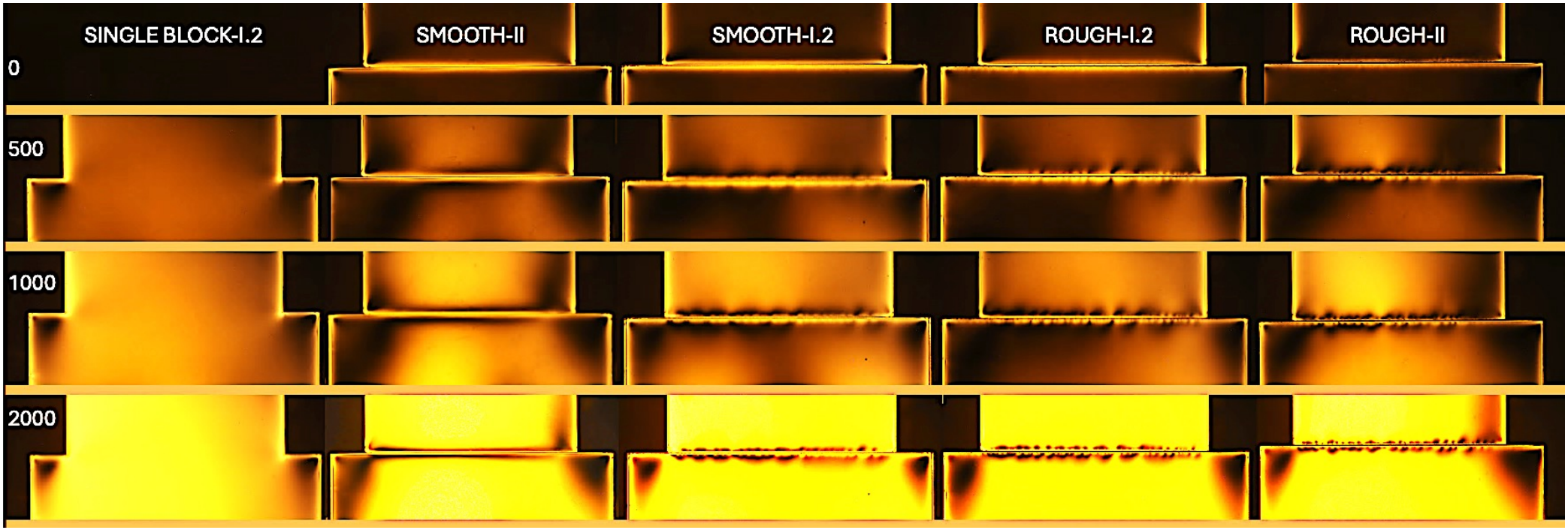

- Rough vs. smooth interfaces produce qualitatively different fringe patterns.
- Collection of asperities create localized stress concentrations that are visible as fringe pattern heterogeneities.

Strain Distributions (Exy) using Digital Image Correlation (DIC): Non-uniform shear strain distribution under normal loading

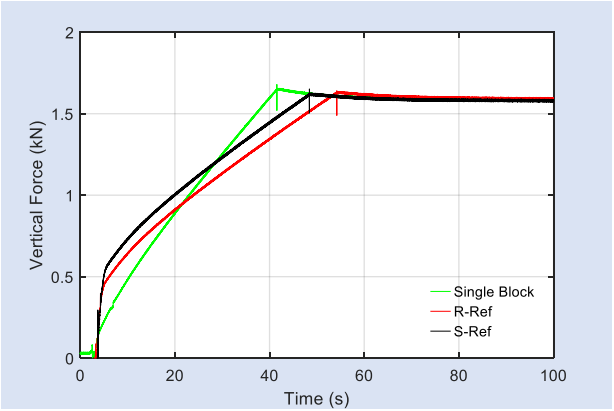

	First Frames of Normal Loading :N<<Nmax	Final Frame of Normal Loading: N=Nmax
Single Block	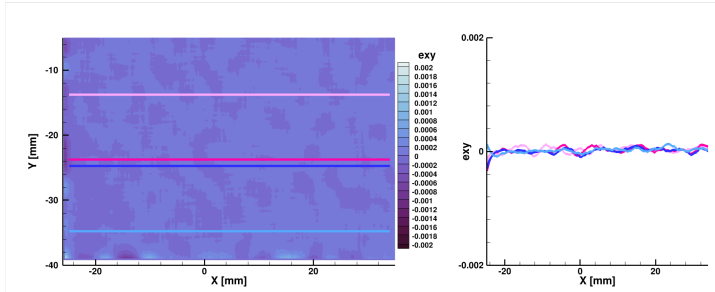	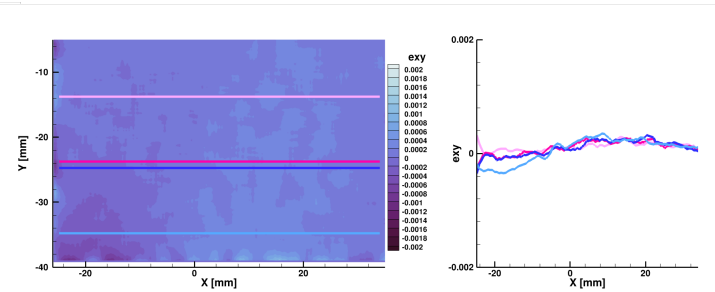
Rough Interface	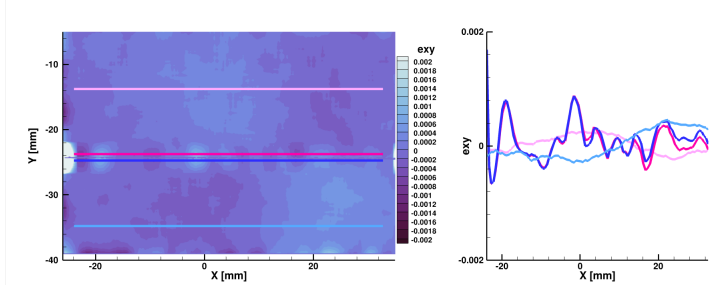	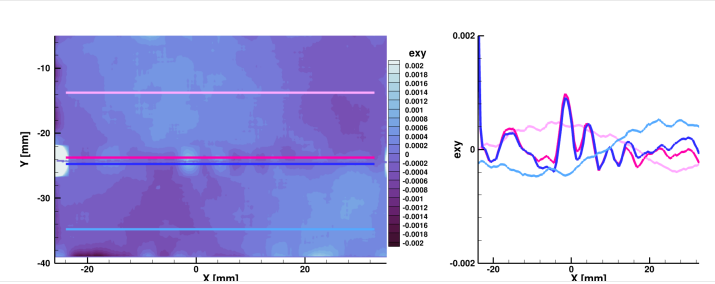
Smooth Interface	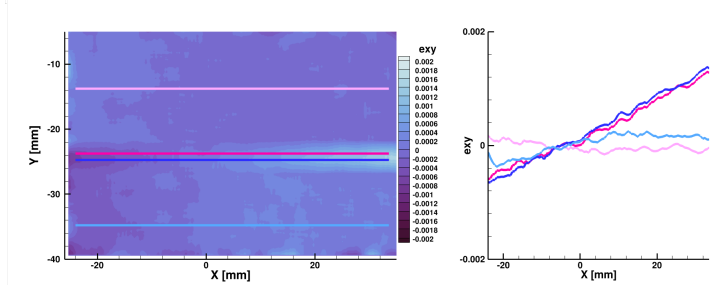	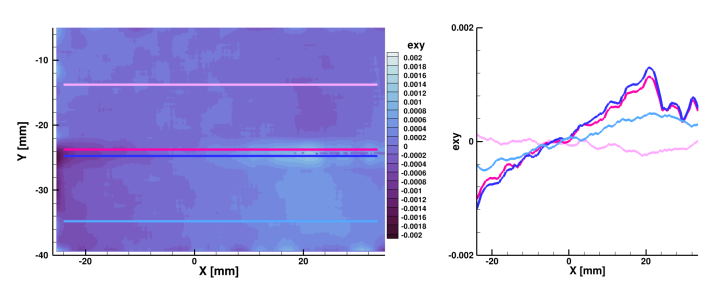

Strain Distributions (Exx) using Digital Image Correlation (DIC): Non-uniform shear strain distribution under shear loading

In addition to the normal load, shear load was applied with no sliding

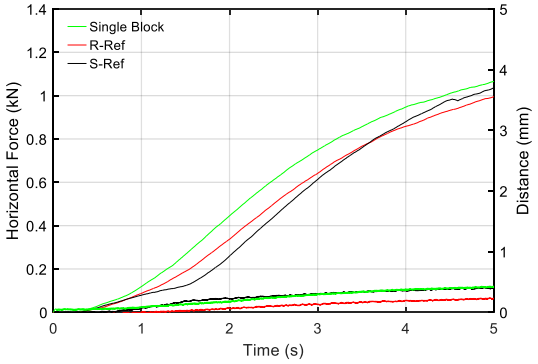

	First Frames of Shear Loading :S<<Smax	Final Frame of Shear Loading: S=Smax
Single Block	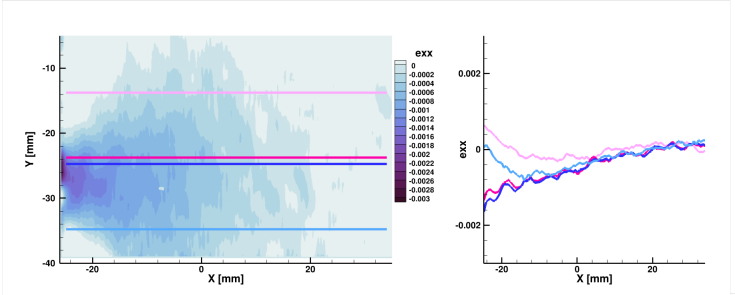	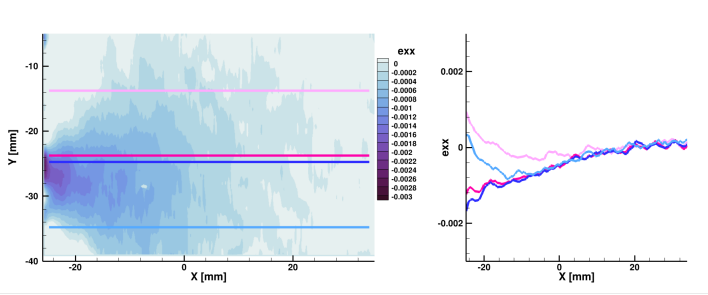
Rough Interface	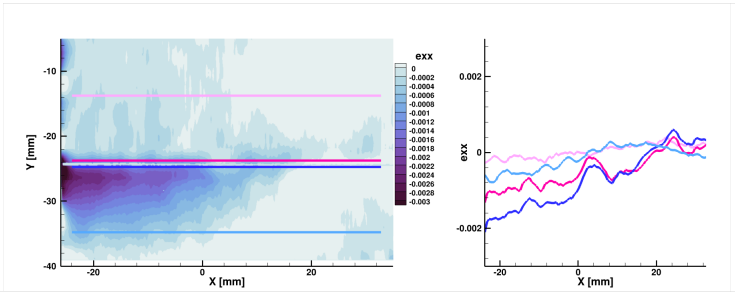	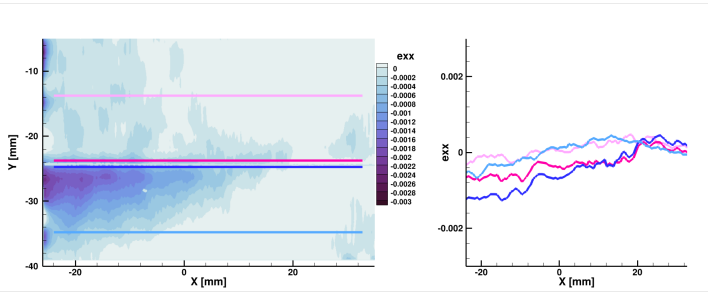
Smooth Interface	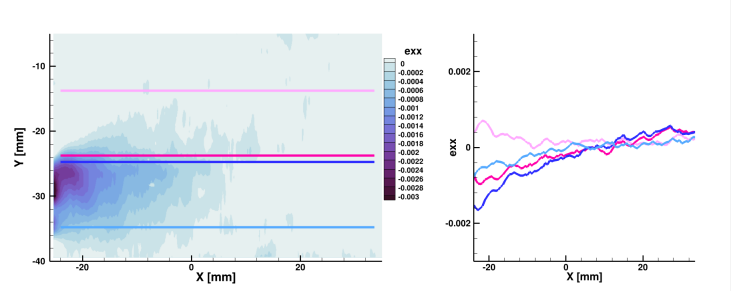	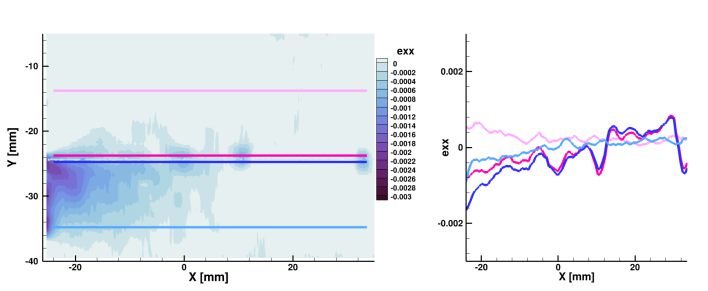

Experimental Method: The setup and the test procedure

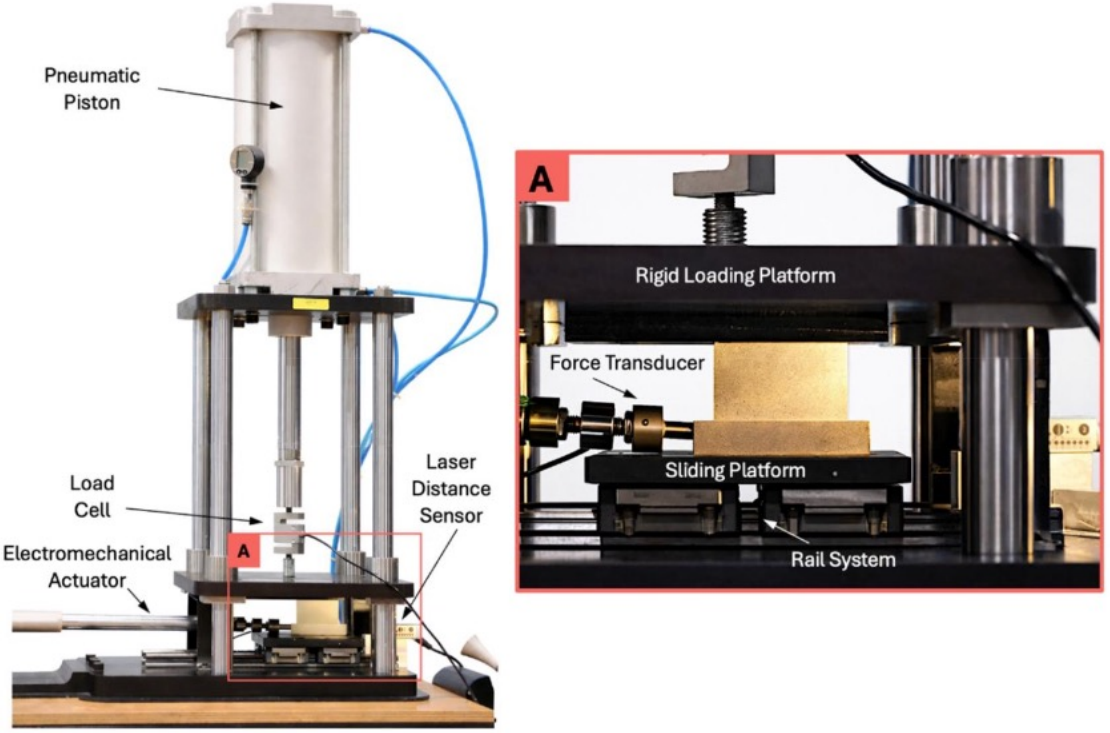

Figure 1. Frictional test setup. Frictional test setup showing the complete loading frame with the pneumatic piston, load cell, electromechanical actuator and laser distance sensor. Inset shows a close-up of the test section, including the force transducer, rigid loading platform, sliding platform and rail system used to position the PMMA plate couple.

Baygeldi, Amireghbali, Gurel, Ozcan, Coker (*Mech. Adv. Mater. Struct.,* 2026)

Experimental Method: The setup and the test procedure

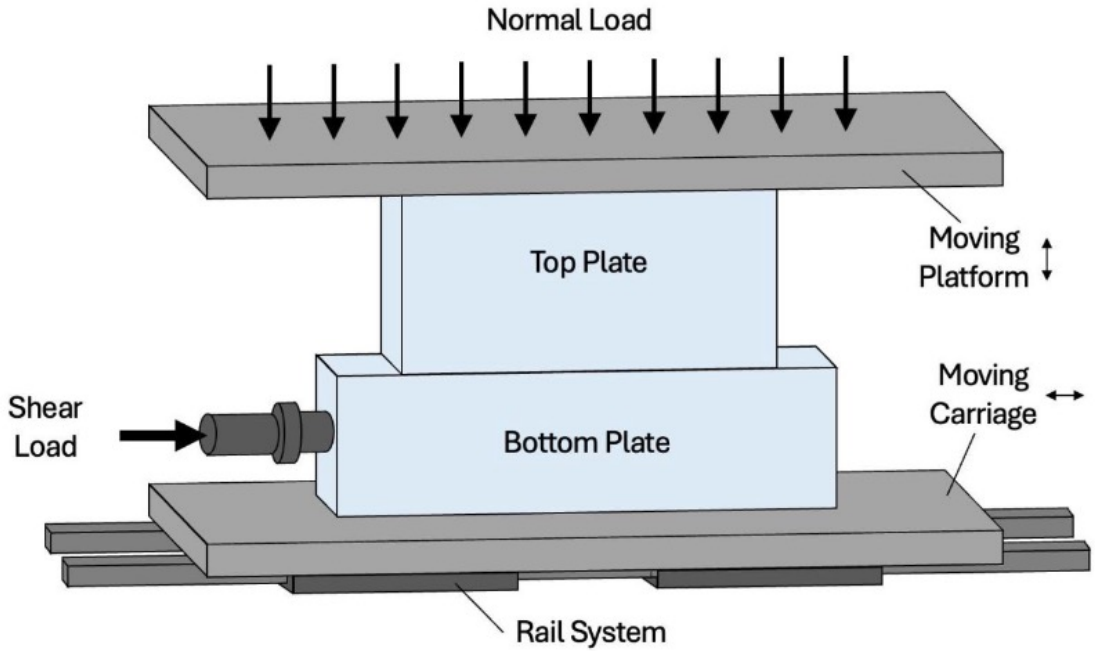

Figure 2. Schematic of the PMMA specimen couple positioning for frictional sliding experiments. A distributed uniform normal load is applied to the top plate through the moving platform, while a shear load is applied to the bottom plate. The bottom plate is mounted on a carriage that moves along a rail system, enabling relative sliding between the mating PMMA surfaces.

Experimental Method:
The setup and the test procedure

$$R_a = \frac{1}{L}\int_0^L |z(x)|dx$$

Table 1. Surface roughness of PMMA plates for different surface preparation techniques.

Surface Preparation Technique	R_a (μm)
Polished (P4000)	0.023
Diamond Saw-Cut	0.296
Laser-Cut	0.840
Polished(P40)	4.108

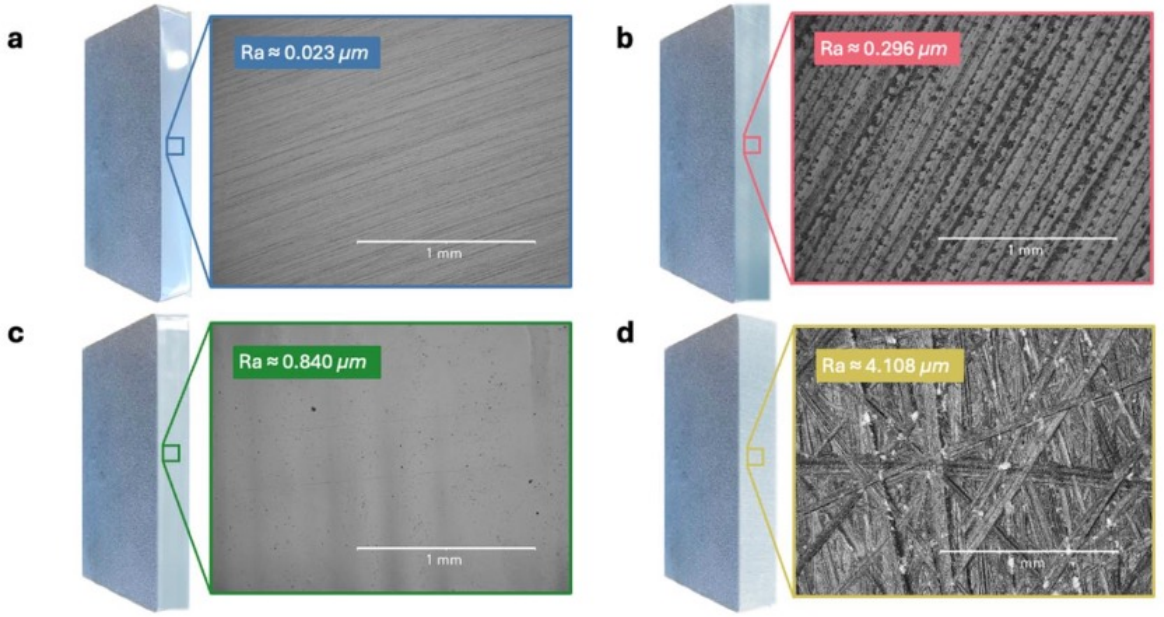

Figure 3. Surface topography of PMMA blocks. Optical microscope images of the PMMA surfaces prepared using (a) 4000 P sandpaper ($R_a \approx 0.023\ \mu m$), (b) diamond-saw cutting ($R_a \approx 0.296\ \mu m$), (c) laser cutting ($R_a \approx 0.840\ \mu m$), and (d) 40 P sandpaper ($R_a \approx 4.108\ \mu m$). Scale bars, 1 mm.

Experimental Results:
Surface Roughness as a Critical Parameter for Frictional Sliding Instability

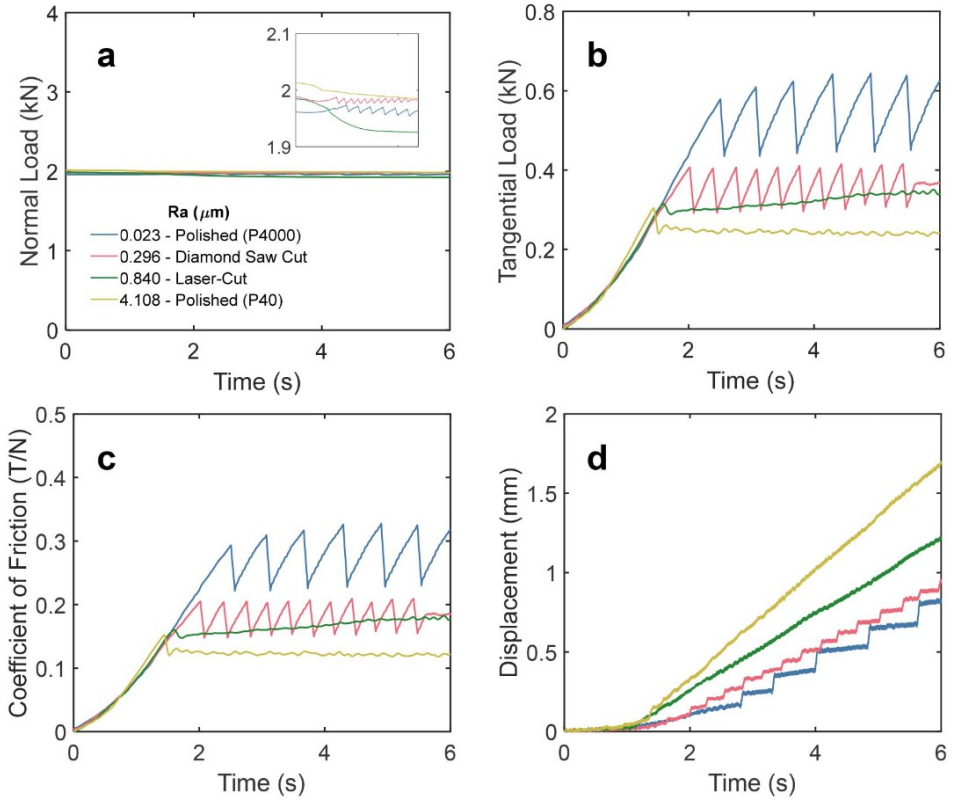

Figure 4. Experimental results showing the effect of surface roughness on frictional sliding behavior, transitioning from steady sliding to stick-slip with decreasing roughness. The time evolution of (a) normal load, (b) tangential load, (c) coefficient of friction, and (d) relative displacement is presented.

Baygeldi, Amireghbali, Gurel, Ozcan, Coker (*Mech. Adv. Mater. Struct.*, 2026)

Mass-spring model to simulate «creeping/ locked fault» dynamics

The Burridge-Knopoff model

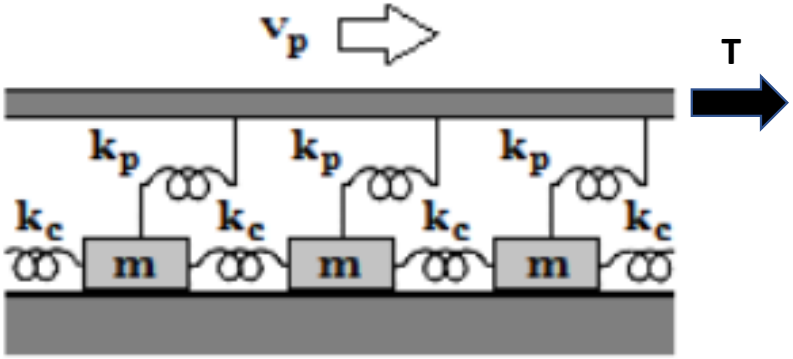

Maxwell-slip model

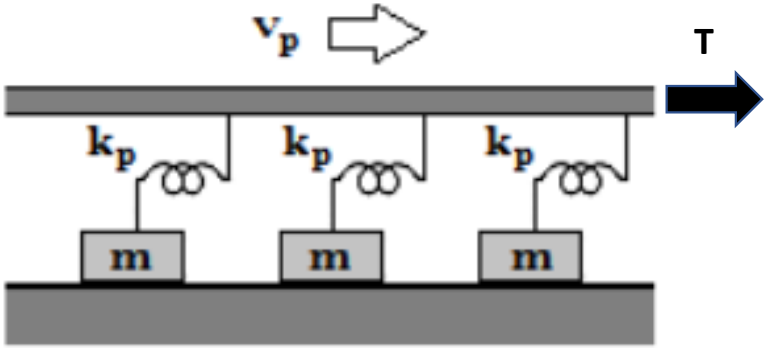

Maxwell-slip model in control engineering: Modelling Friction

Artificial muscles

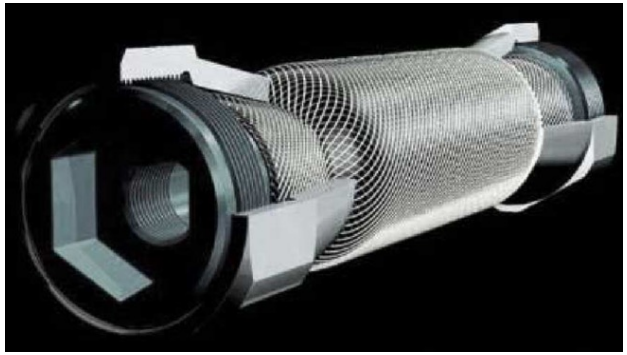

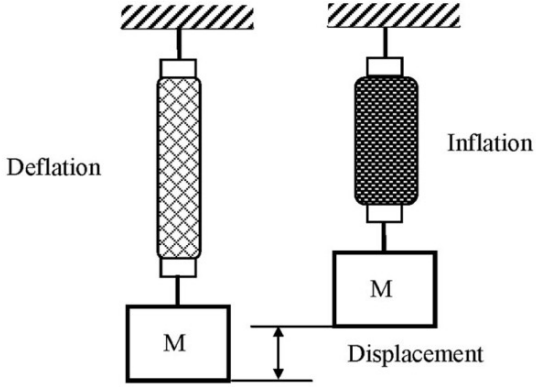

Vo-Minh, Tjahjowidodo, Ramon, & Van Brussel (*IEEE*, 2011)

Machining tools

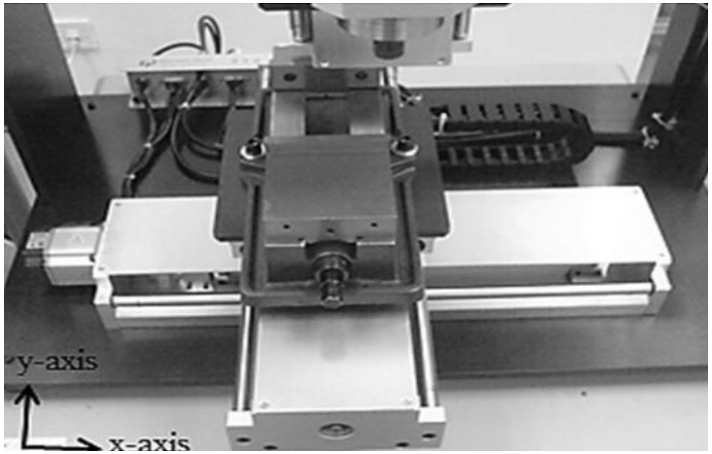

Chiew, Jamaludin, Bani, Hashim, Rafan, & Abdullah (*Procedia Engineering,* 2003)

Accurate position control

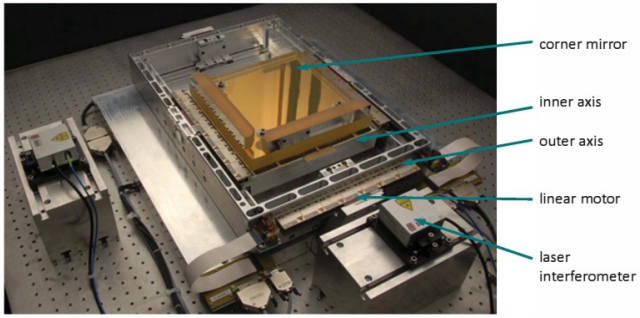

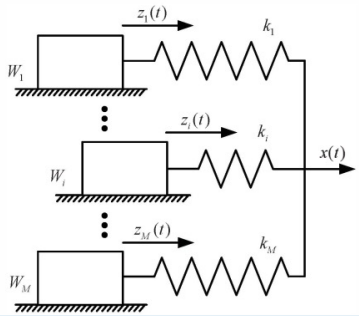

Zschack, Buchner, Amthor, & Ament (*IEEE*, 2012)

Simple 1-D modeling of stick slip vs. steady sliding behavior

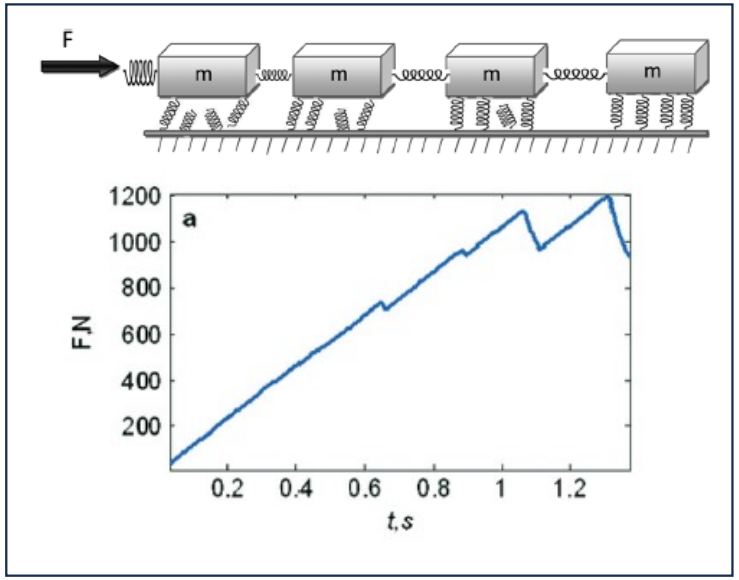

Braun, Barel, and Urbakh
(*Physical Review Letters*, 2009)

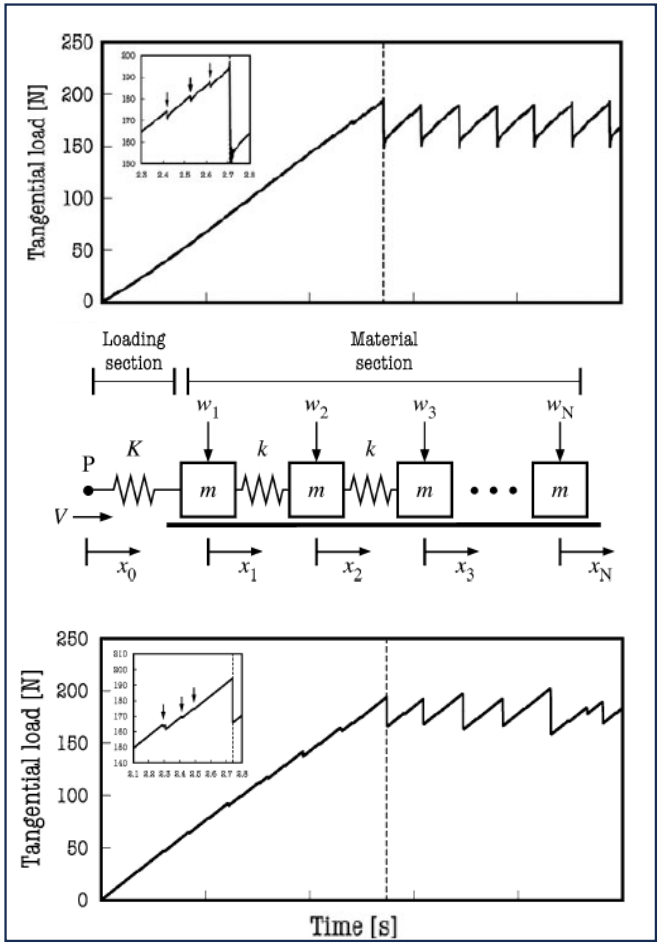

Maegawa, Suzuki, and Nakano
(*Tribology Letters*, 2010)

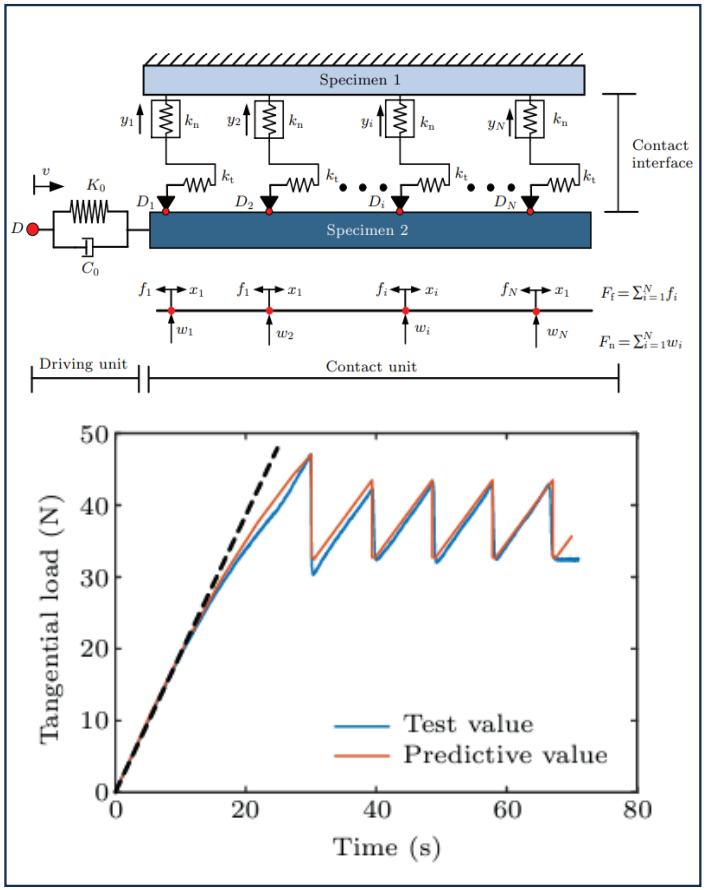

Han, Ding, Wu, and Yan
(*Chinese Physical B*, 2022)

Simple 1-D modeling of asperities to generate rate- and state-friction model

Hulikal, Bhattacharya, Lapusta (*JMPS*, 2015)

- Interface represented as a population of viscoelastic spring-dashpot elements, each representing an asperity contact
- Hulikal et al. (2015): showed that macroscopic rate-and-state friction behavior emerges from collective dynamics of viscoelastic asperities
- Velocity weakening arises naturally from the statistical evolution of the asperity population — not prescribed at the element level
- Hulikal et al. (2018): extended the model to study the effect of asperity-scale properties and long-range interactions
- Frictional behavior across static, transient, and steady sliding is governed by the balance between time-dependent strengthening and slip-induced weakening
- Key insight: macroscopic friction laws are emergent properties, not fundamental constitutive equations

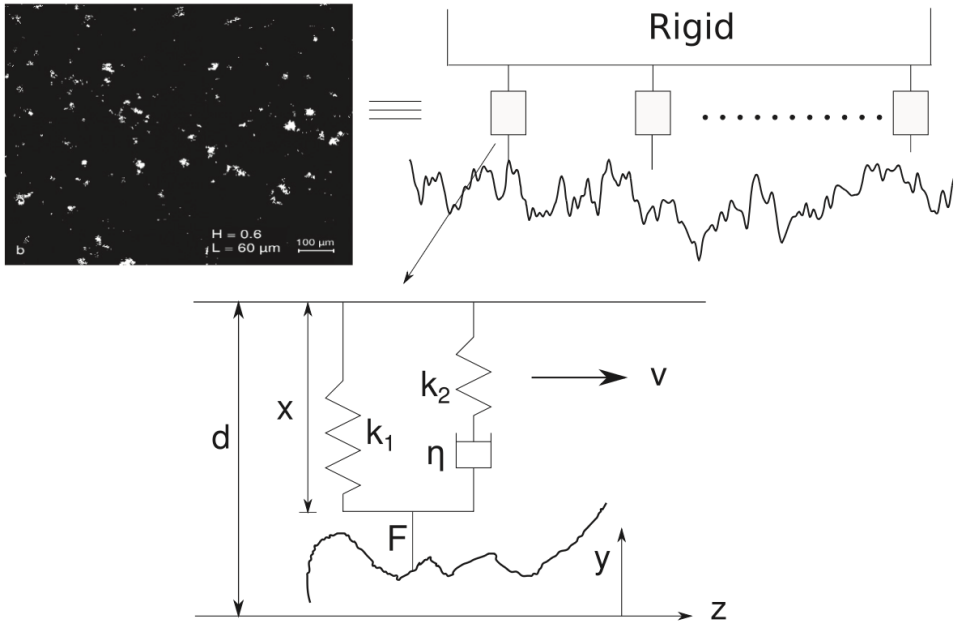

1D Minimal Maxwell Slip Model: Modelling the Roughness Effect

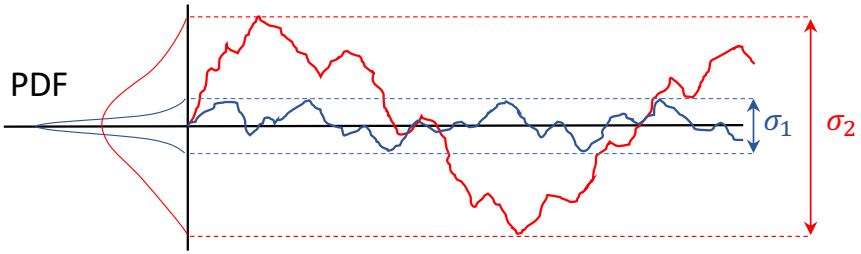

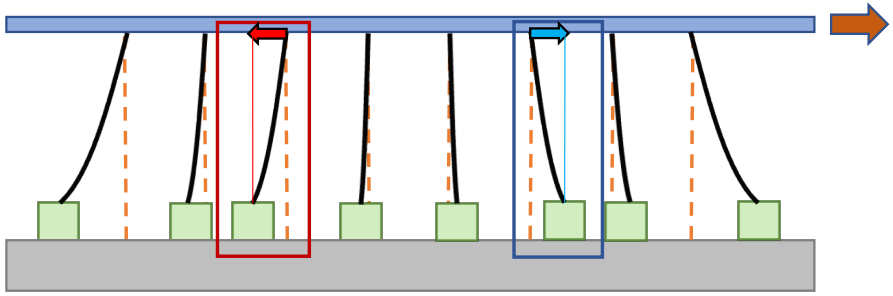

The initial block positions before the driver moves

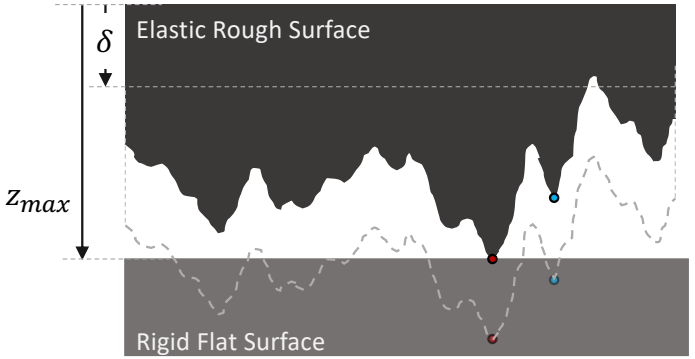

The initial spring extensions of the blocks are interpreted as a measure of roughness

- The higher asperities experience higher compressive loads, so they will slide later. This is modeled as a mass-spring with positive displacement.
- The lower asperities experience lower compressive loads, so they will slide earlier. This is modeled as a mass-spring with negative displacement.

Baygeldi, Amireghbali, Gurel, Ozcan, Coker (*Mech. Adv. Mater. Struct.*, 2026)

Numerical Method: Modelling the Roughness Effect
Generation of Random Initial Spring Extensions

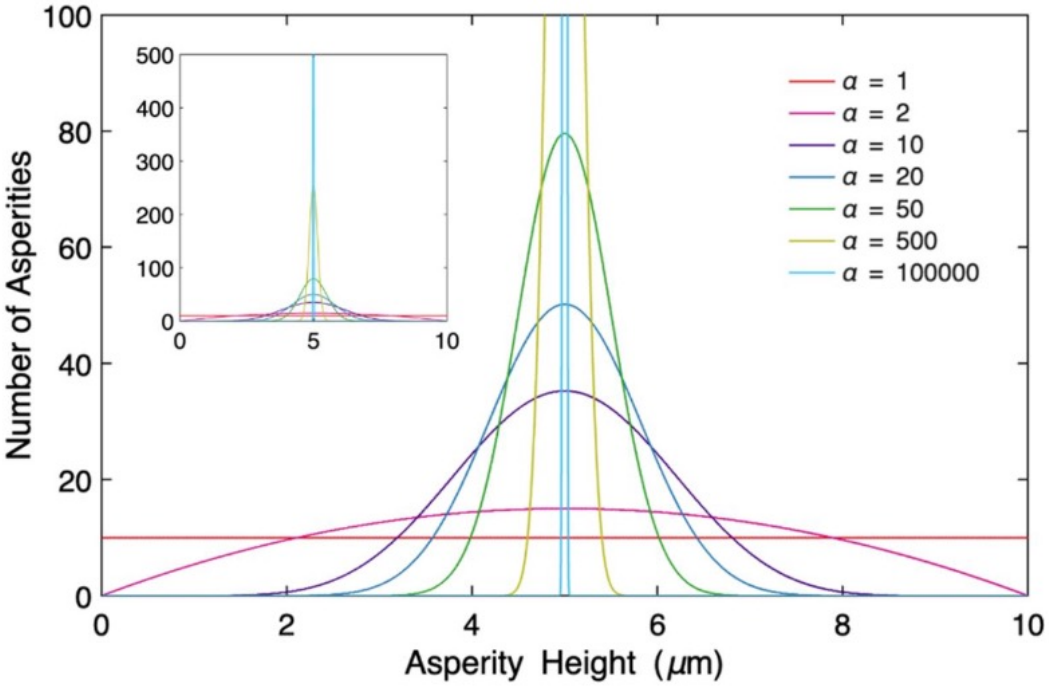

Beta probability distribution function with shape parameters $\alpha = \beta$ is used.

$$\sigma = \frac{1}{2}\sqrt{\frac{1}{2\alpha + 1}}$$

- The rougher surfaces are modeled with a larger standard deviation of spring extensions with smaller shape parameter, α.
- The smoother surfaces are modeled with a smaller standard deviation of spring extensions with larger shape parameter, α.

Numerical Method: Modelling the Roughness Effect
1D Minimal Maxwell-slip Model: Quasi-static Solution

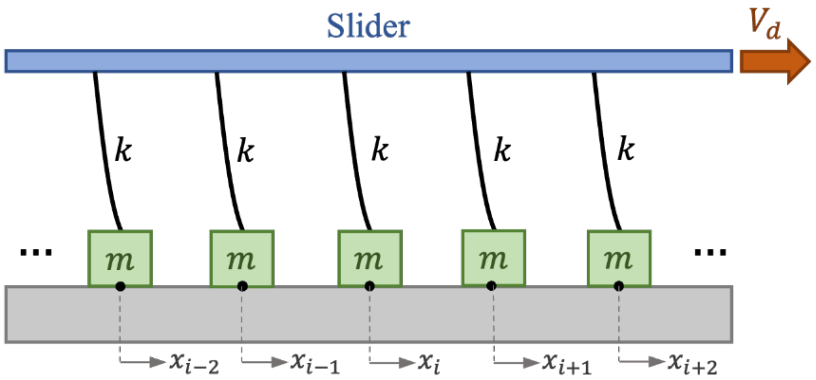

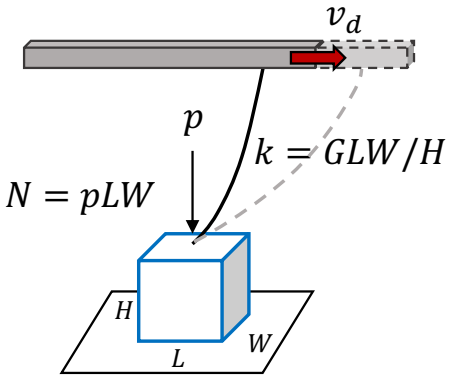

$f_{th} = \mu_s N$

Stick

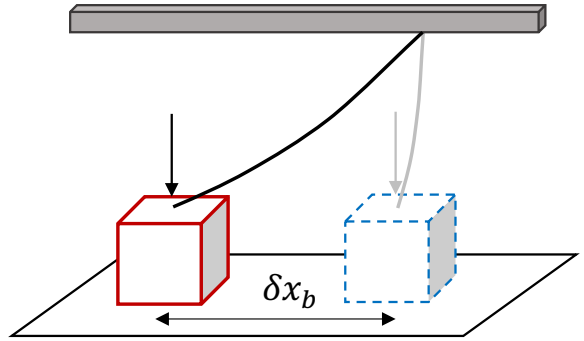

$f_d = \mu_d N$

Sliding Stick

Maxwell-slip model:

- Coulomb friction law
- Quasi-static approach

$$m\ddot{x} = f_{sp} - f_{fr} = k(v_d t_d - x) - f_{fr}$$

$$\delta x_b = 2\frac{\mu_s - \mu_d}{k} N_b$$

Numerical Results: Modelling the Roughness Effect

Maxwell-slip Model: Quasi-static Solution

Stick-slip Regime

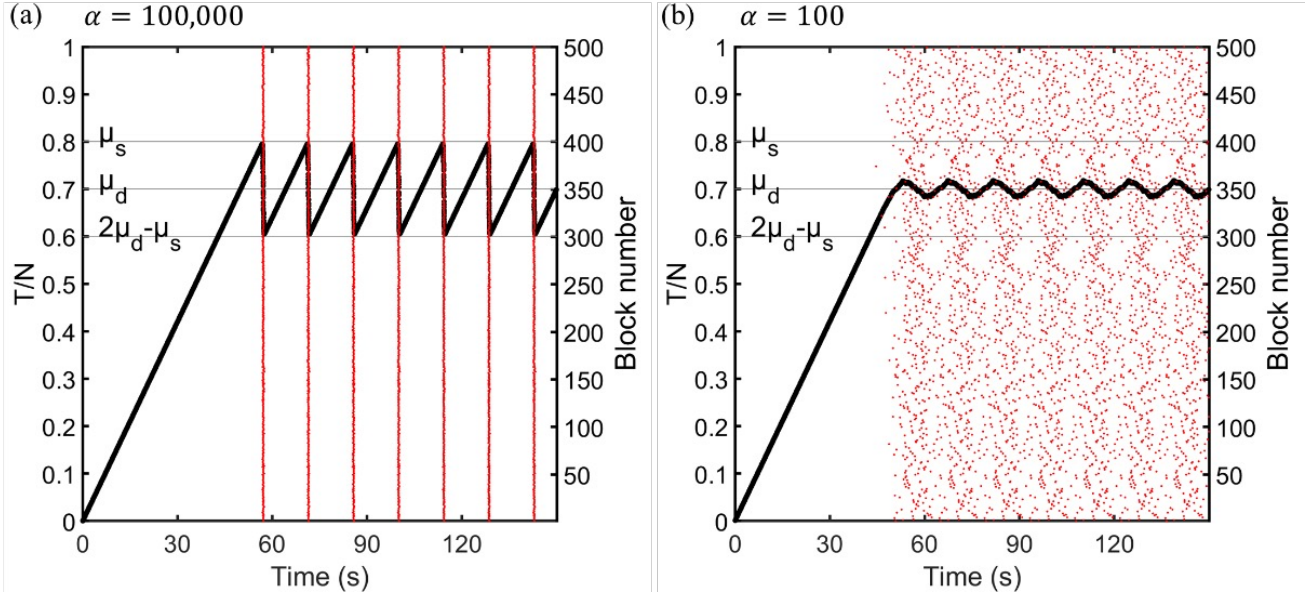

- **Macroscopic** coefficient of friction, T/N, rises and falls about the **microscopic** dynamic coefficient of friction, μ_d.
- Presliding regime is linear.
- Amplitudes of stick-slip oscillations decrease with decreasing α, i.e., surface gets rougher.

Numerical Results: Modelling the Roughness Effect

Maxwell-slip Model: Quasi-static Solution

Stick-slip Regime

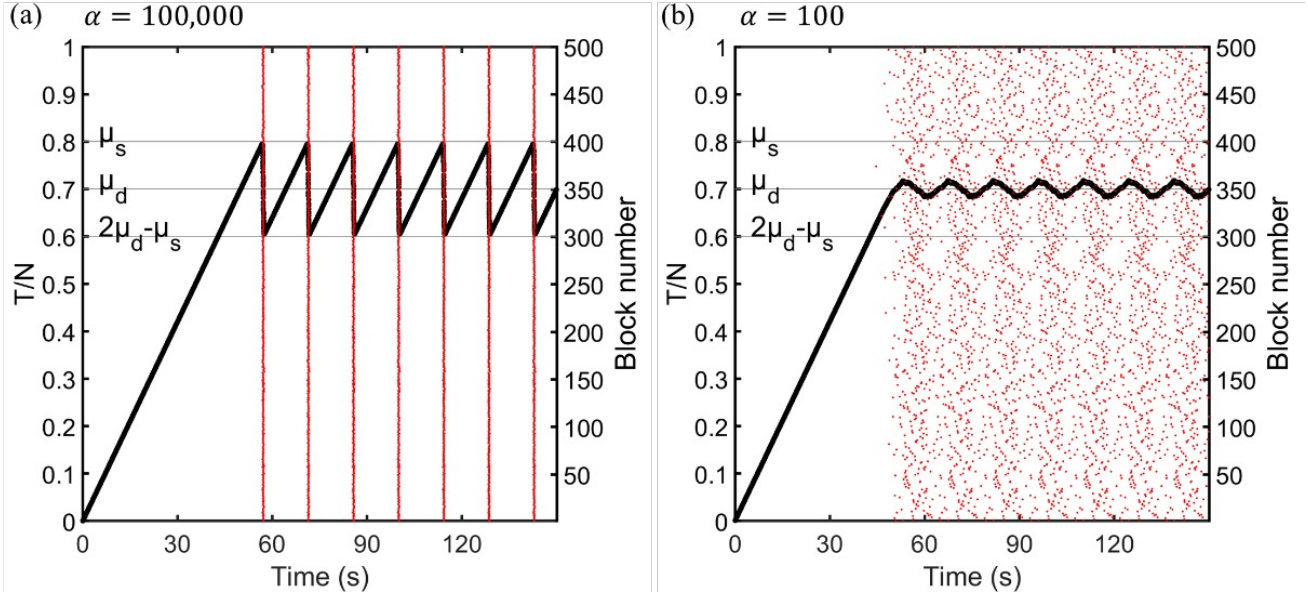

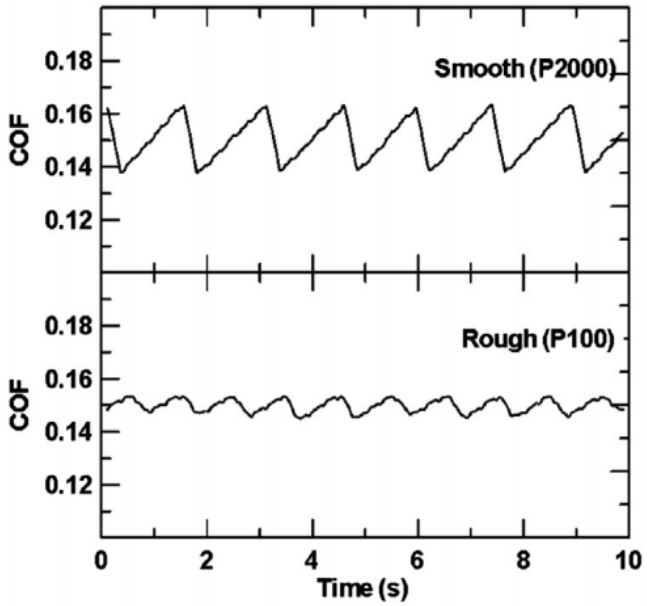

Lee S M, Shin M W, Lee W K and Jang H (*Wear*, 2013)

Numerical Results: Modelling the Roughness Effect

Maxwell-slip Model: Quasi-static Solution

Steady Sliding Regime

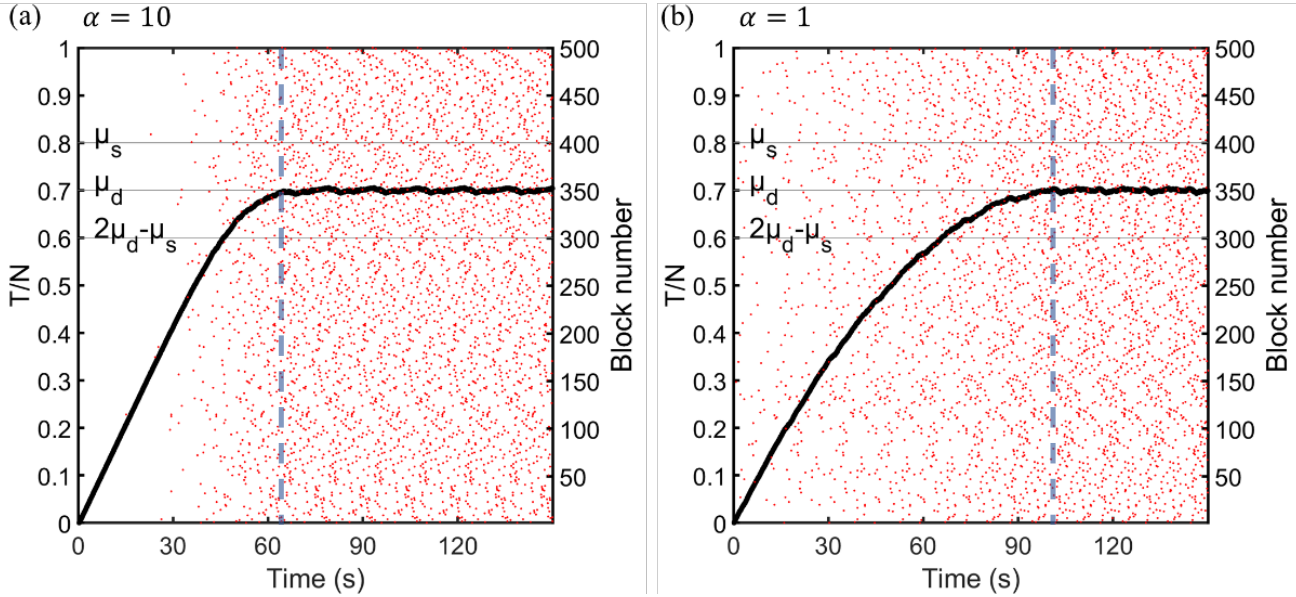

- **Macroscopic** coefficient of friction, T/N, approaches the **microscopic** dynamic coefficient of friction, μ_d, and stays there.
- Presliding regime becomes nonlinear with decreasing α, i.e. surface gets rougher.
- Onset of sliding starts later for rougher surface.

Numerical Results: Modelling the Roughness Effect

Maxwell-slip Model: Quasi-static Solution

Steady Sliding Regime

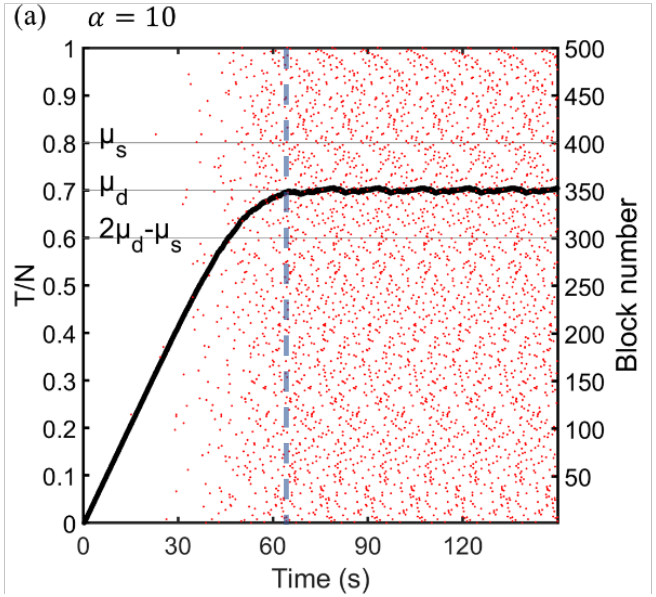

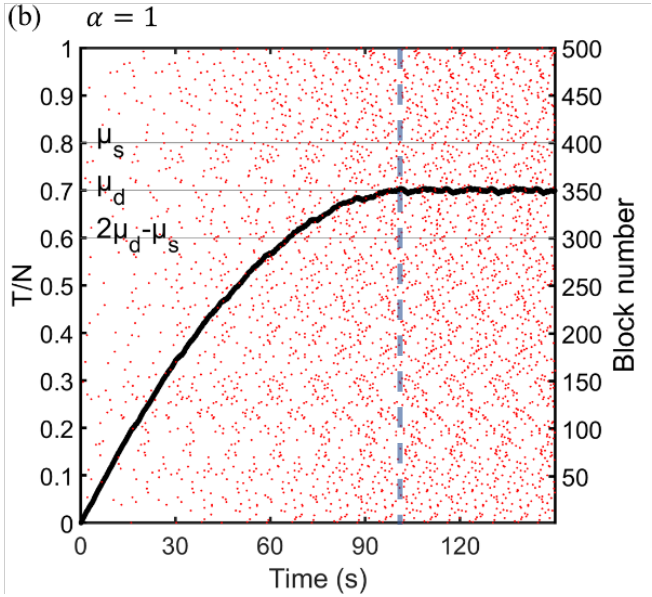

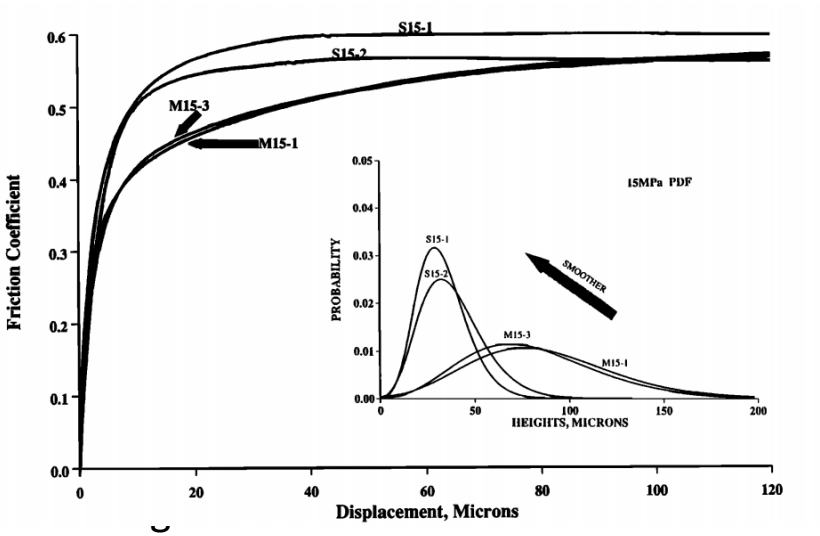

Biegel R L, Wang W, Scholz C H, Boitnott G N and Yoshioka N, Journal of Geophysical Research (1992)

Baygeldi, Amireghbali, Gurel, Ozcan, Coker (Mechanics of Adv. Matls. & Structures, 2026)

Results: How does maximum static COF change with roughness?

Two different regimes of sliding!

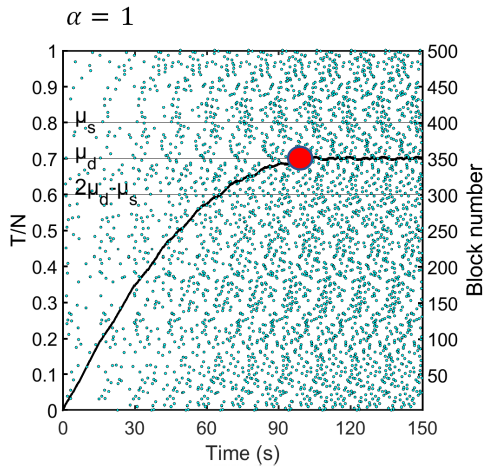

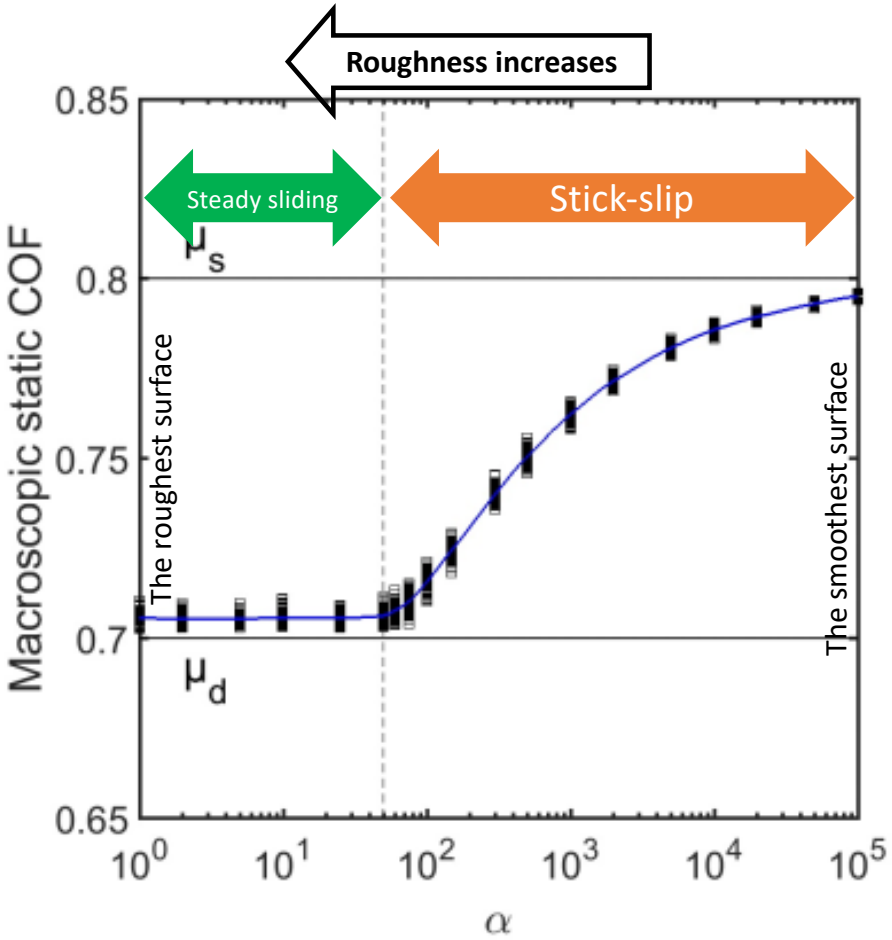

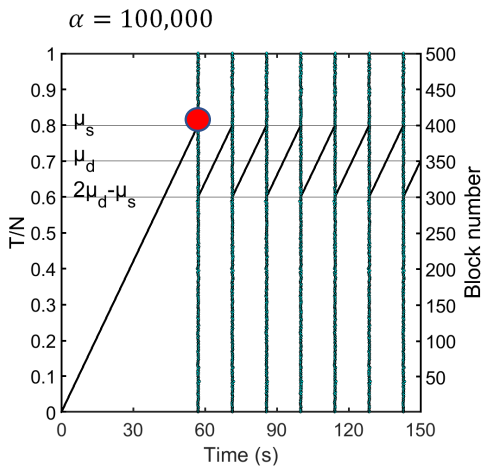

Microscopic friction coefficients are constant — the macroscopic behavior emerges from the ensemble statistics.

Experiments and Maxwell Slip Model

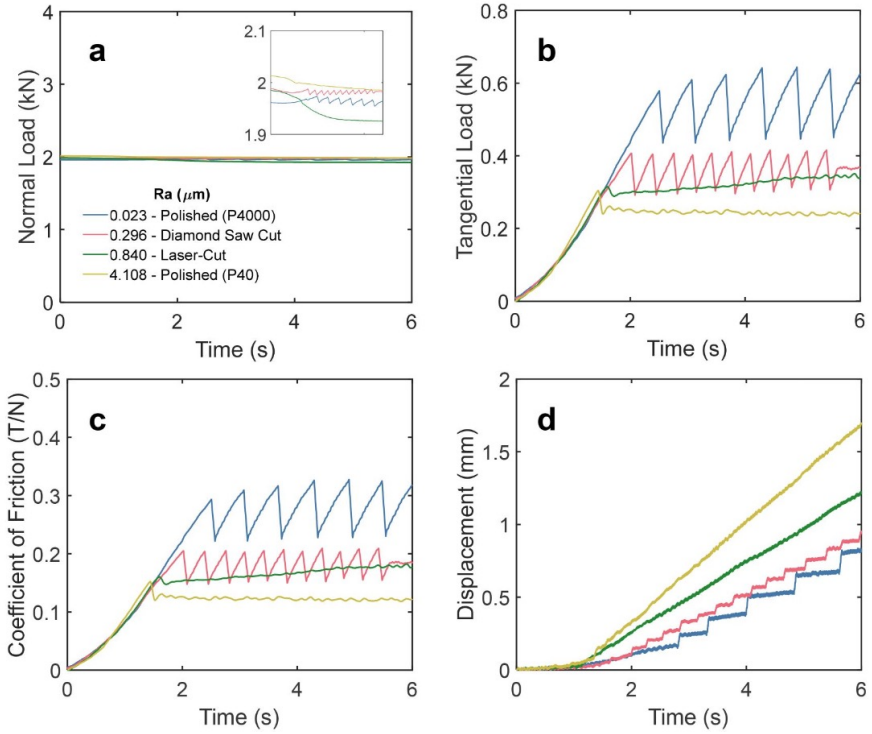

Figure 4. Experimental results showing the effect of surface roughness on frictional sliding behavior, transitioning from steady sliding to stick-slip with decreasing roughness. The time evolution of (a) normal load, (b) tangential load, (c) coefficient of friction, and (d) relative displacement is presented.

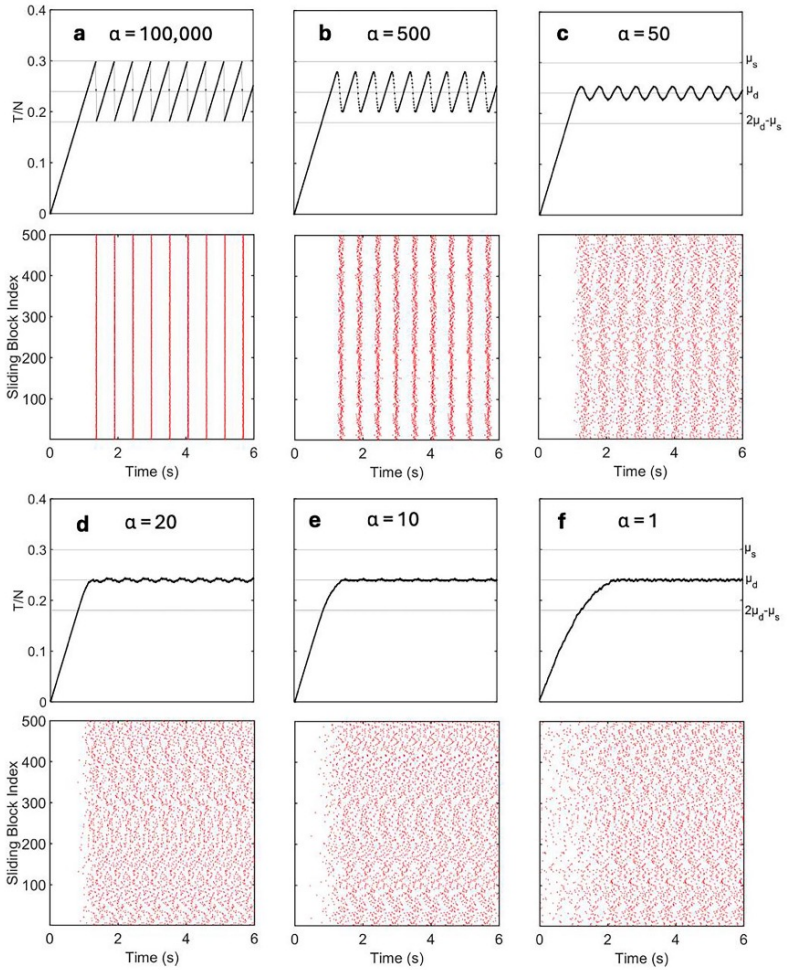

igure 9. The results of the quasi-static approach adapted to the Maxwell-slip model for six different random initial block position distributions. Time evolution of the macroscopic CoF and the slipped block index numbers (the red dots) are presented. The shape parameter of the beta probability distribution, α, for each case are respectively: (a) = 100,000 (b) α = 500 (c) α = 50 (d) α = 20 (e) α = 10, and (f) α = 1. The case (a) corresponds to the smoothest surface, and the case (f) corresponds to the roughest surface.

Baygeldi, Amireghbali, Gurel, Ozcan, Coker, "Surface Roughness as a Critical Parameter for Frictional Sliding Instability: Experiments and Modeling (*Mech. Adv. Mater. Struct.*, 2026)

From Model to Experiments: Critical Roughness

–Standard deviation of surface height distribution:

$$\sigma = \frac{\mu_s p h}{G\sqrt{2\alpha + 1}}$$

–Relationship between α and R_a:

$$R_{a,\,crit} = \frac{2\mu_s p_e h}{G\sqrt{\pi(2\alpha_c + 1)}}$$

using effective contact pressure $p_e = p/f$ (Greenwood–Williamson framework)

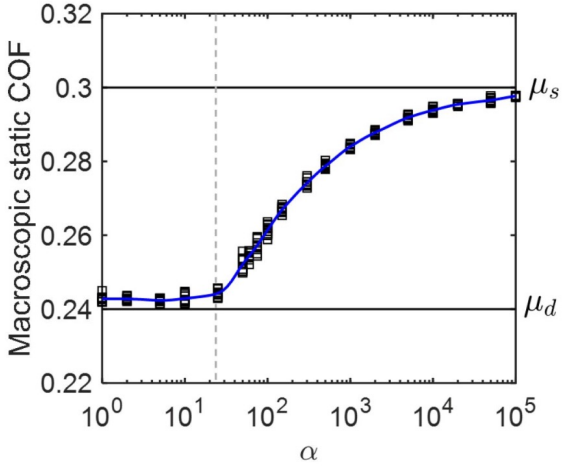

Figure 10. Macroscopic static CoF value evolution with roughness. The black square markers represent the macroscopic static CoF values obtained from 100 runs for each beta distribution function shape parameter, α. The blue line is a curve fit to the mean value obtained for each of the α values. The vertical dashed line at $\alpha = 22$ delineates a border between steady sliding regime on its left and stick-slip regime on its right. The microscopic static and dynamic CoF values are plotted as horizontal lines.

- Real contact area fraction: f ≈ 1.1–1.5% → effective pressure significantly exceeds nominal pressure
- With $\alpha_c = 22$, $\mu_s = 0.3$, h = 0.05 mm, G = 1.1 GPa: critical roughness $R_{a,crit} \approx 0.408–0.557$ µm
- Experimental transition lies between $R_a \approx 0.296$ µm and $R_a \approx 0.840$ µm —agreement with model prediction , $R_{a,crit}$.
- Validation on independent dataset: Bouissou et al. (1998) at 10 MPa — α-R_a mapping correctly classifies their stick–slip and steady sliding cases.

Physical Interpretation of the Transition

- The critical α separates two fundamentally different modes of microscopic sliding dynamics:
- Below α_c (rough): asperities have widely distributed initial states → they slip at different times → the average force remains steady → steady sliding
- Above α_c (smooth): asperities have nearly identical initial states → they reach the friction threshold simultaneously → collective failure → stick–slip
- The transition is sharp — not gradual — indicating a threshold-type behavior analogous to a phase transition
- Surface roughness provides the disorder that desynchronizes asperity slip; below a critical level of disorder, synchronization emerges spontaneously
- This framework provides a mechanistic link: microscale interface disorder → asperity slip synchronization → ensemble macroscopic sliding stability

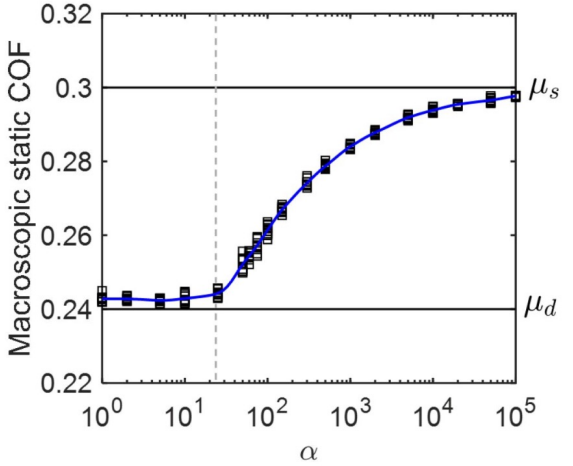

Figure 10. Macroscopic static CoF value evolution with roughness. The black square markers represent the macroscopic static CoF values obtained from 100 runs for each beta distribution function shape parameter, α. The blue line is a curve fit to the mean value obtained for each of the α values. The vertical dashed line at $\alpha = 22$ delineates a border between steady sliding regime on its left and stick-slip regime on its right. The microscopic static and dynamic CoF values are plotted as horizontal lines.

Collective vs. Sequential Asperity Slip

- Each asperity contact acts as an independent frictional element that can slip when its local threshold is exceeded
- Smooth surface: narrow distribution of thresholds → all asperities reach threshold nearly simultaneously → collective slip
- Rough surface: broad distribution of thresholds → asperities slip at different times → sequential slip
- Collective slip produces macroscopic stick–slip; sequential slip produces macroscopically steady sliding
- This is the mechanism captured by the Maxwell-slip ensemble model — roughness controls the synchronization of slip events
- The transition is sharp: below a critical disorder parameter, collective slip emerges; above it, sequential slip dominates

Stick-Slip Regime –> Rupture Initiation and Front Propagation

The slip part seems to occur almost spontaneously.
In fact, slip occurs dynamically as a time dependent rupture at a scale of microseconds.

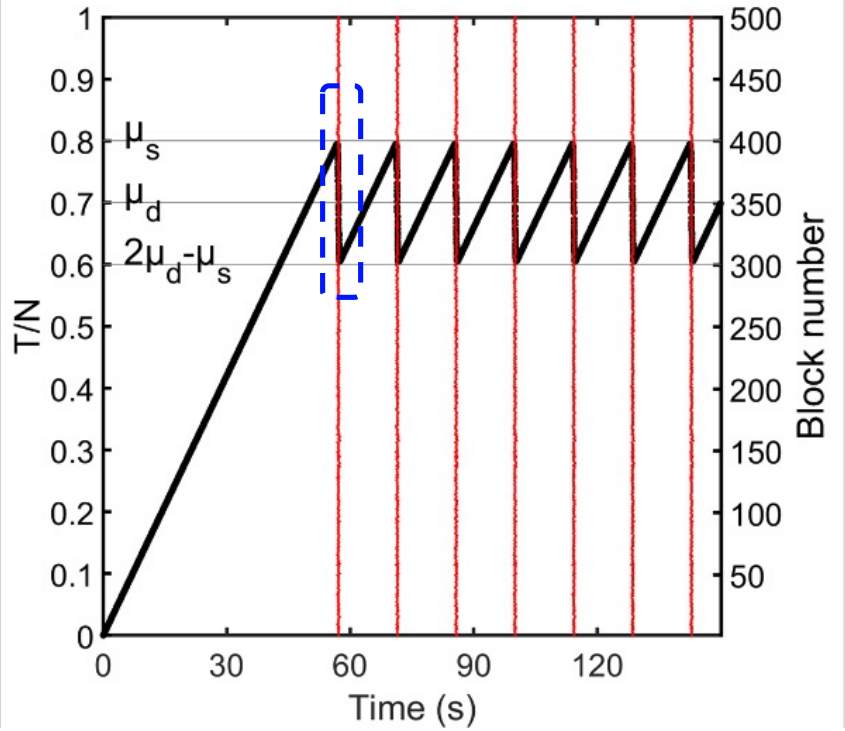

Stick–slip involves propagation of rupture fronts along the interface — analogous to dynamic fracture (Trømborg et al., 2011)

Smooth interfaces: low nucleation barrier → rupture can propagate coherently across the entire interface → large stress drop

Rough interfaces: roughness increases the effective nucleation size → disrupts coherent propagation (Harbord et al., 2017)

Precursor events: partial slip fronts extend progressively before full macroscopic sliding initiates (Maegawa et al., 2010)

The number and extent of precursors depend on normal stress distribution, which is itself affected by roughness

Our minimal model does not capture rupture propagation explicitly, but the collective-to-sequential transition is consistent with this picture

PART 2

Rupture Front Propagation

Dynamic frictional sliding along interfaces between identical materials

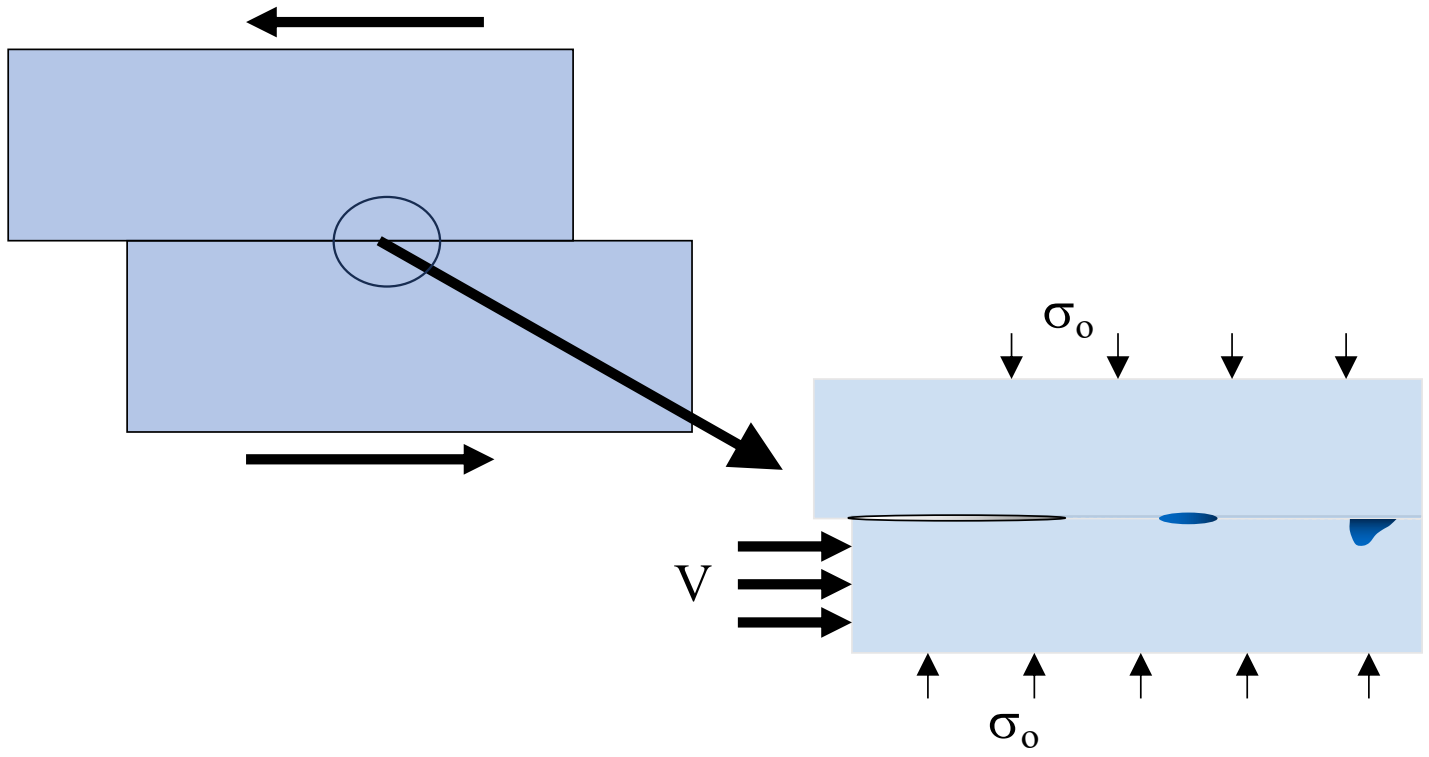

Modeling of friction across length-scales

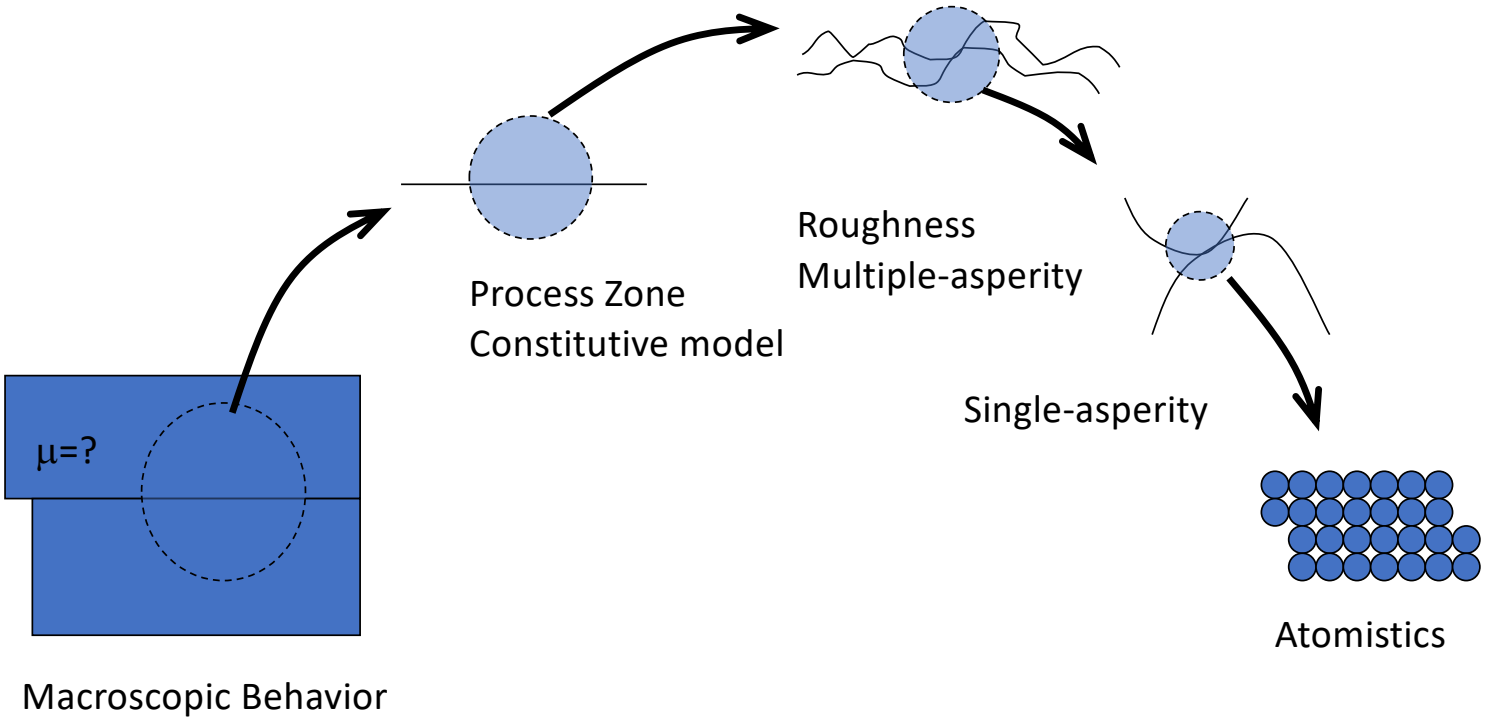

Fiber Pull-Out Experiments (K-S Kim)

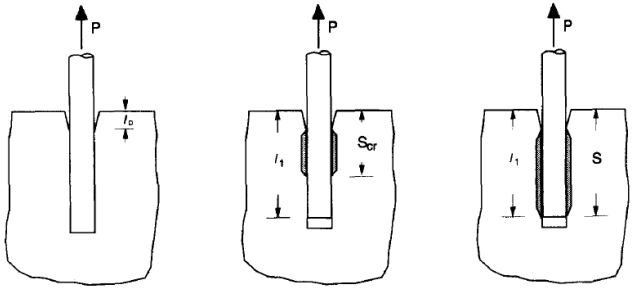

(i) Precursor of fiber pull-out: Semi-brittle debonding.

(ii) Fiber pull-out with limited active sliding zone. ($S_{cr} < l_1$)

(iii) Fiber pull-out with full active sliding zone. ($S_{cr} > l_1$)

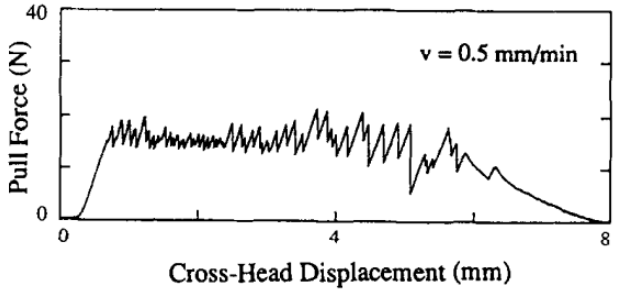

Tsai & Kim (*JMPS*, 1996)

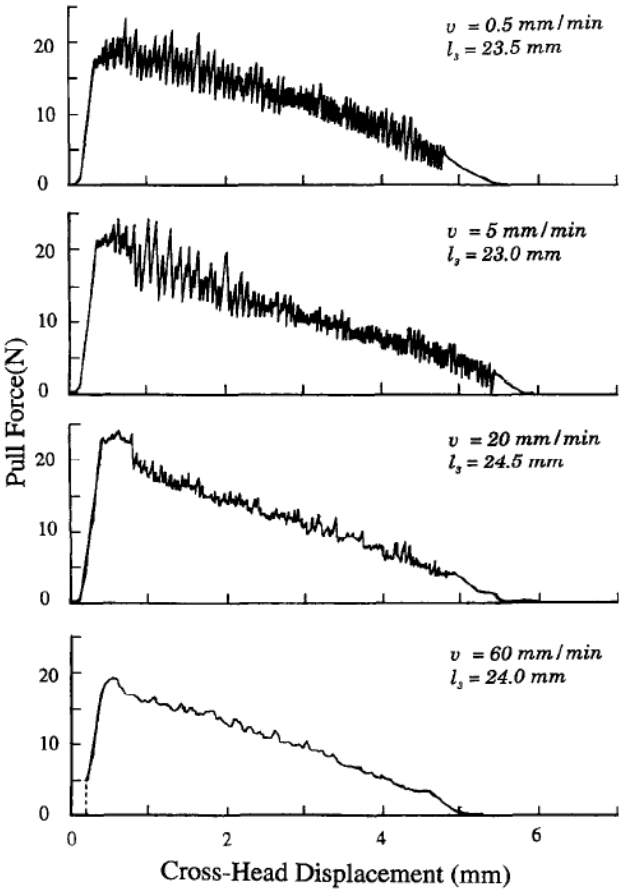

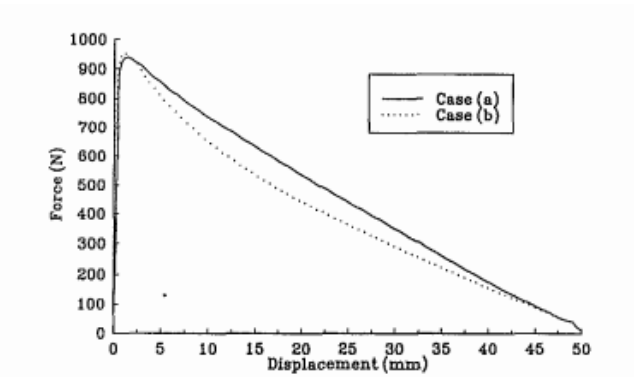

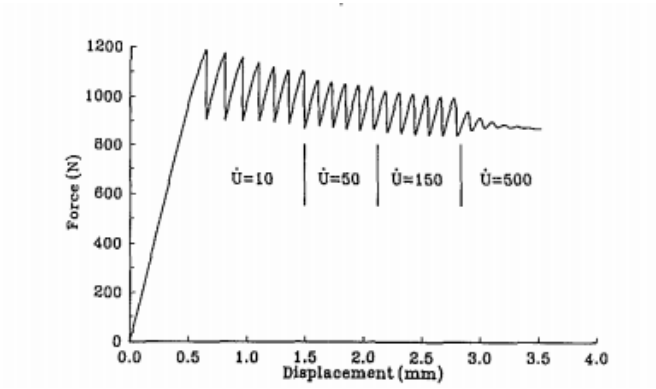

Povirk & Needleman (*JEMT*, 1993)

Slip pulses inferred in earthquakes during frictional sliding of plates

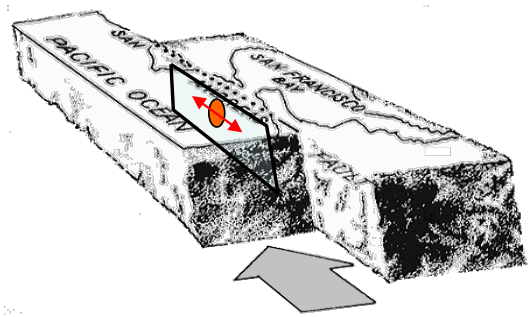

(Heaton, 1990)

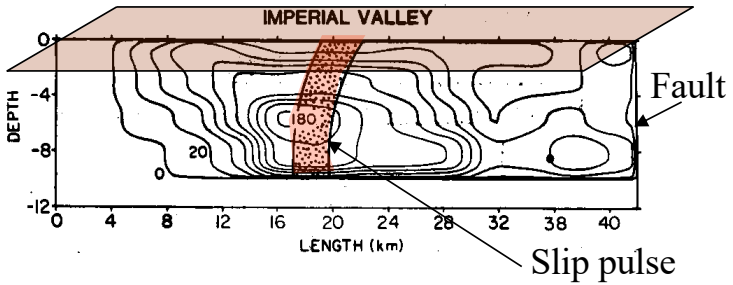

Frictional sliding modes observed in fiber pull-out experiments

Tsai & Kim (*JMPS* ,1996)

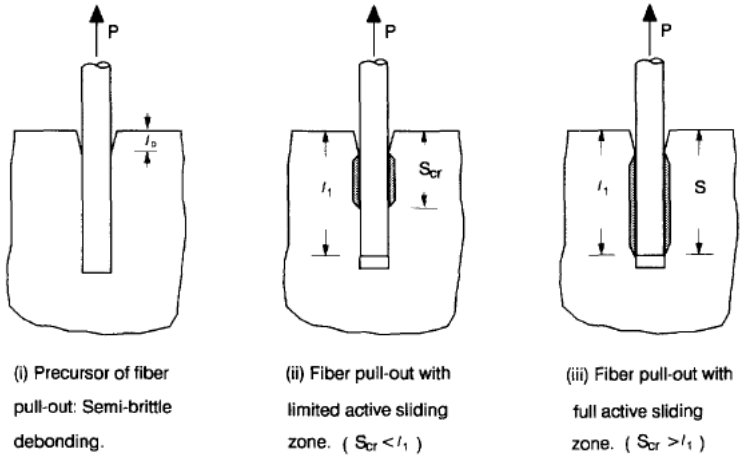

(i) Precursor of fiber pull-out: Semi-brittle debonding.

(ii) Fiber pull-out with limited active sliding zone. ($S_{cr} < l_1$)

(iii) Fiber pull-out with full active sliding zone. ($S_{cr} > l_1$)

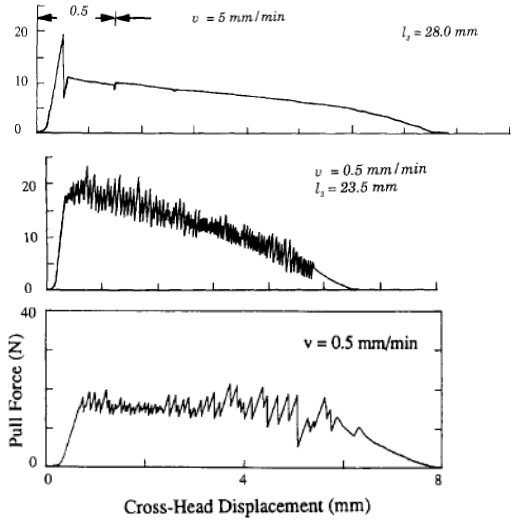

History and sliding speed affect the apparent coefficient of friction

Marone, *Annu. Rev. Earth Planet. Sci. 1998.*

Amontons-Coulomb law: $\tau = \mu \sigma$

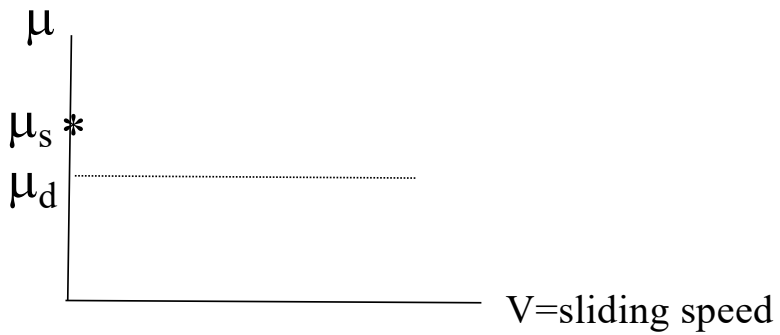

Experiments

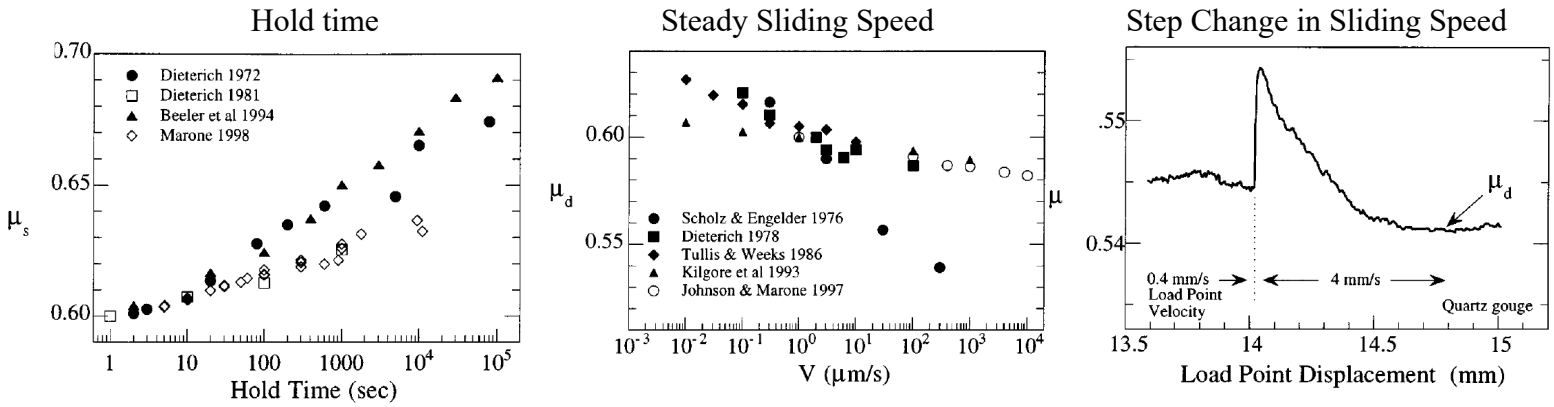

→Amontons-Coulomb friction law is not adequate to capture these phenomena.

Effect of sliding speed on the coefficient of friction for various materials (Dieterich)

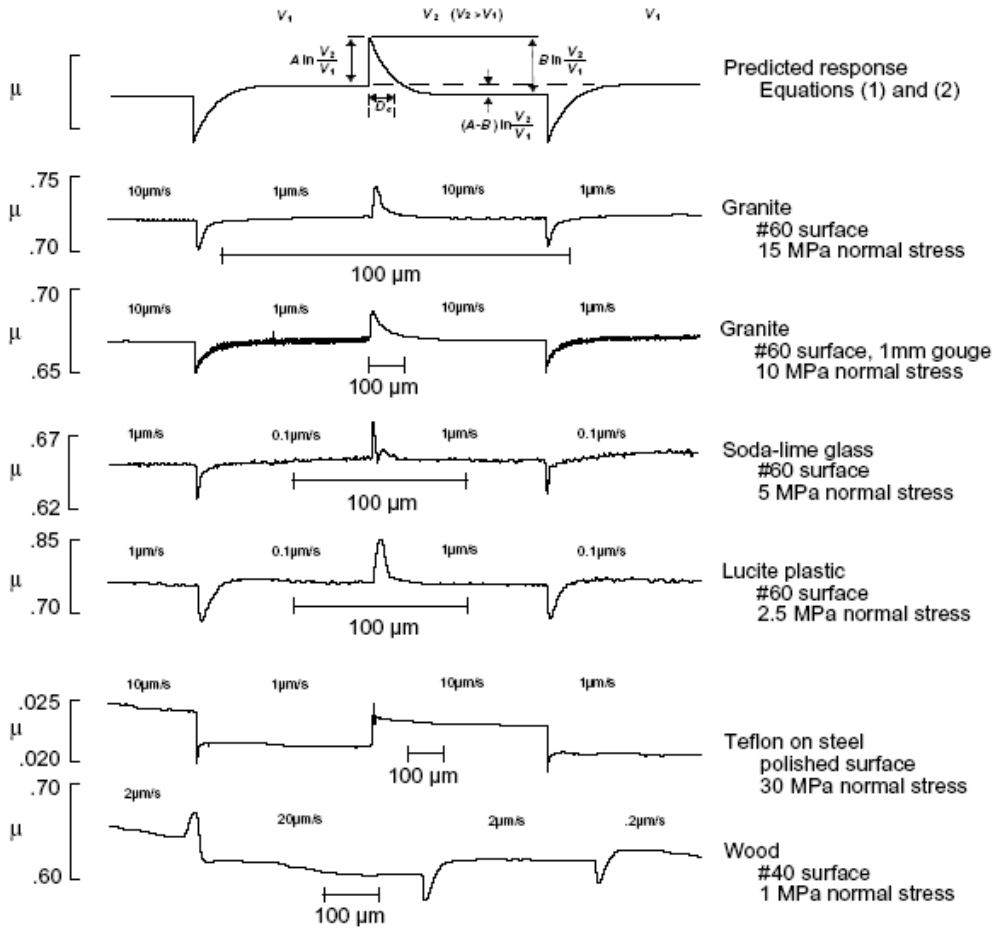

Friction Interface Law: Rate- and state-dependent with variations in normal stress

$$T_s = \mu(\theta_o, \Delta\dot{u}_{slip})\theta_p(T_n)$$

where $\mu(\theta_o, \Delta\dot{u}_{slip}) = g(\theta_o)\left(\frac{\Delta\dot{u}_{slip}}{V_o} + 1\right)^{1/m}$

$$g(\theta_o) = \frac{\mu_d + (\mu_s - \mu_d)\exp\left[\left(\frac{L_o/\theta_o}{V_o}\right)^p\right]}{\left[\frac{L_o/\theta_o}{V_o} + 1\right]^{1/m}}$$

$$\dot{\theta}_o = A_o\left\{1 - \frac{\theta_o \Delta\dot{u}_{slip}}{L_o}\right\}$$

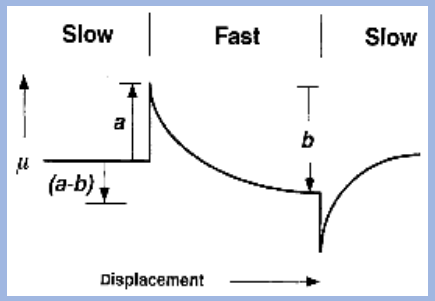

Dieterich, 1979; Ruina, 1983;
Rice and Ruina; 1983

$$\dot{\theta}_p = -\frac{1}{L_p}(\theta_p - DT_n)\Delta\dot{u}_{slip}$$

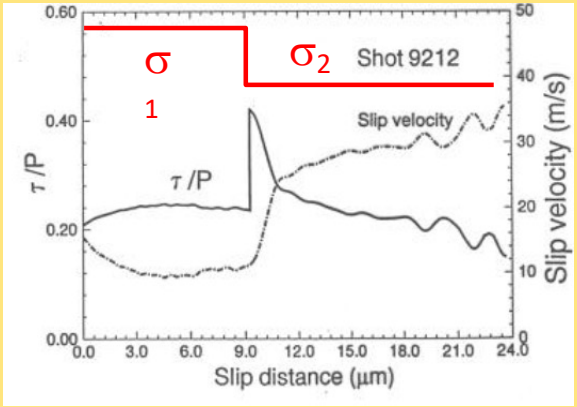

Prakash and Clifton, 1993; Prakash, 1993

Finite element model with friction interface elements in a cohesive framework

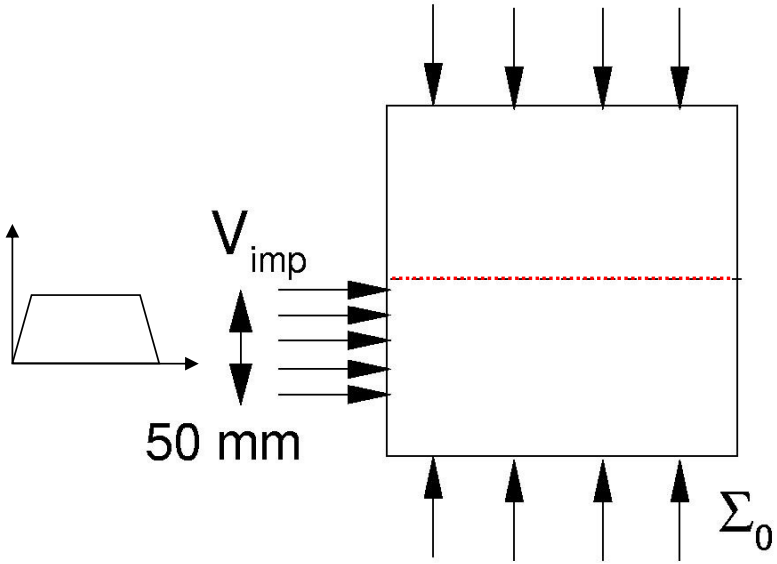

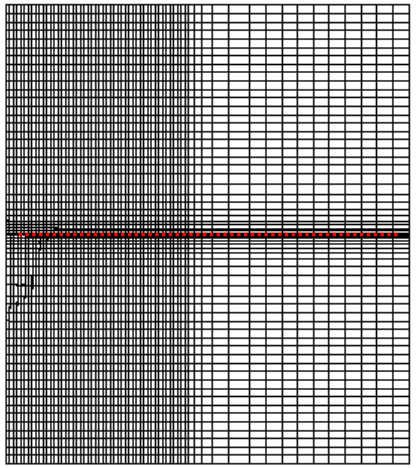

$$\int_V \mathbf{S} : \delta\mathbf{E} dV - \int_{S_{\text{int}}} \mathbf{T} \cdot \delta\Delta\mathbf{u} dS = \int_V \mathbf{T} \cdot \delta\mathbf{u} dV - \int_V \rho : \frac{\partial^2 \mathbf{u}}{\partial t^2} \cdot \delta\mathbf{u} dV$$

$$\dot{T}_n = C_n \Delta\dot{u}_n$$

$$\dot{T}_s = C_s (\Delta\dot{u}_s - \text{sgn}(T_s)\Delta\dot{u}_{slip})$$

(Povirk and Needleman 1993)

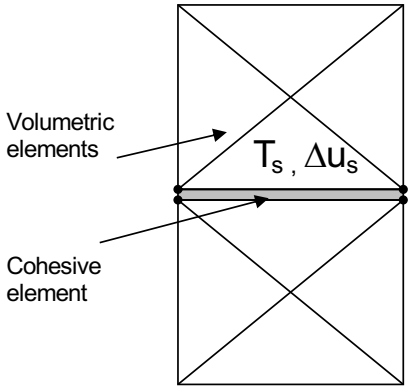

Symmetric loading with no frictional sliding: Experiments and simulations

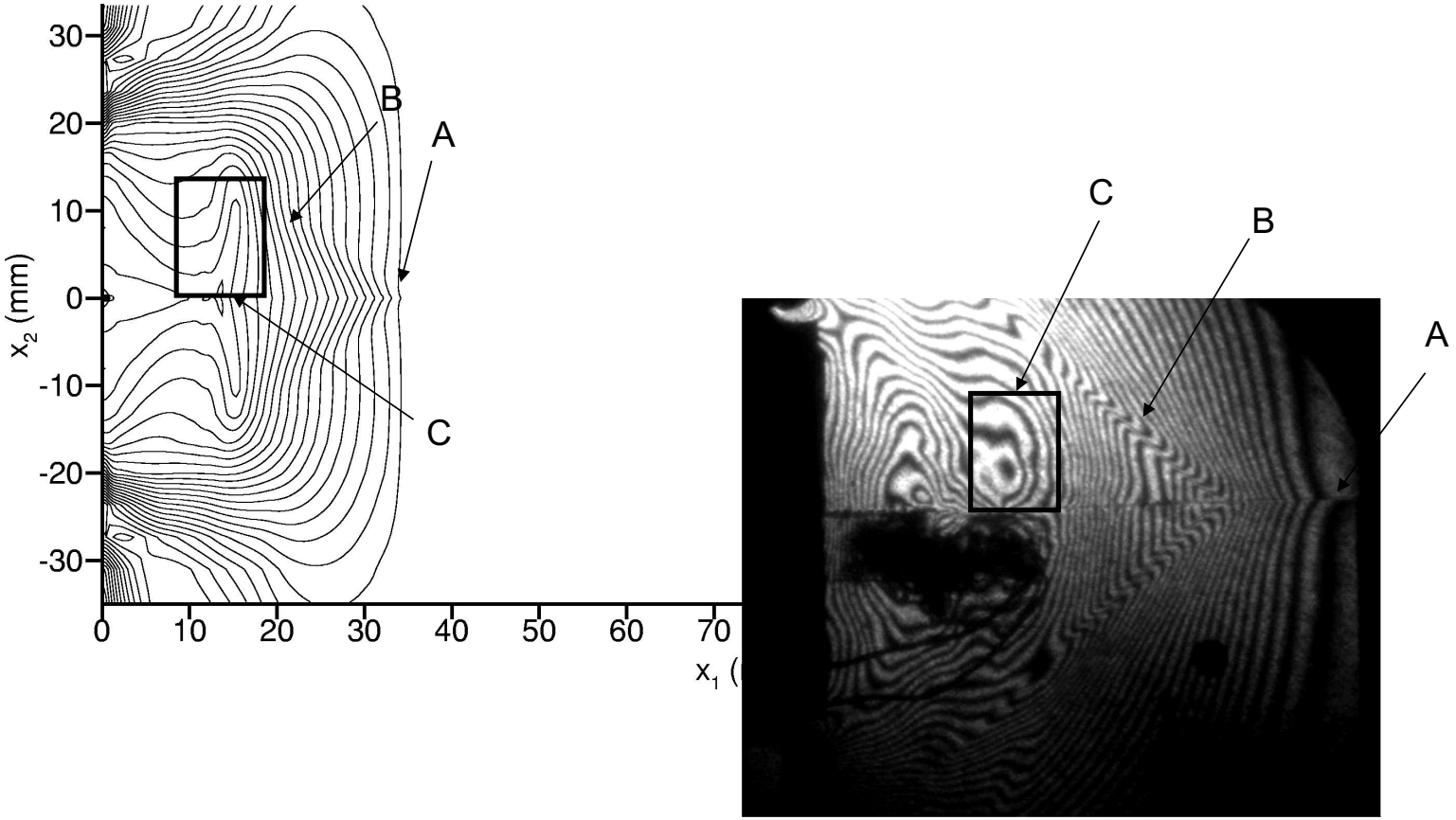

Coker, Lykotrafitis, Rosakis, Needleman (*JMPS*, 2005)

RESULTS

- Case I: Crack-like
- Case II: Slip pulse

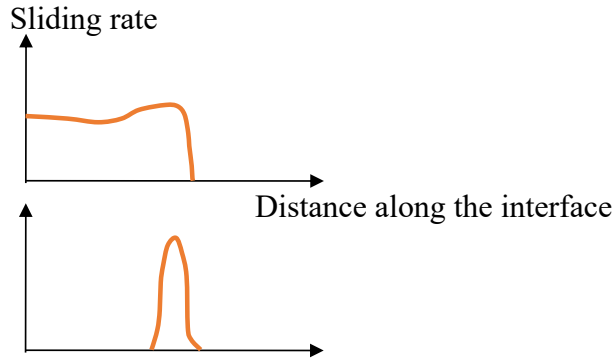

- Case III: Quasi-periodic train of slip pulses
- Case IV: Mixed modes
  - Compare with experiments
- Propagation of frictional sliding tip
- Sliding mode map

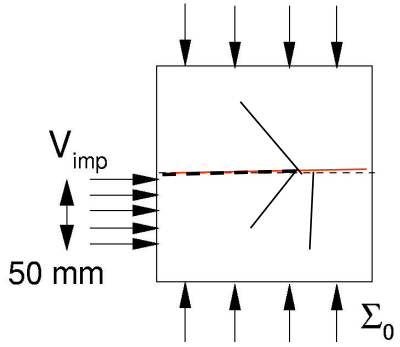

Case I: Results for Σ_o =6 MPa, V_{imp}=2 m/s

At low compressive stress →
Expanding crack-like frictional sliding

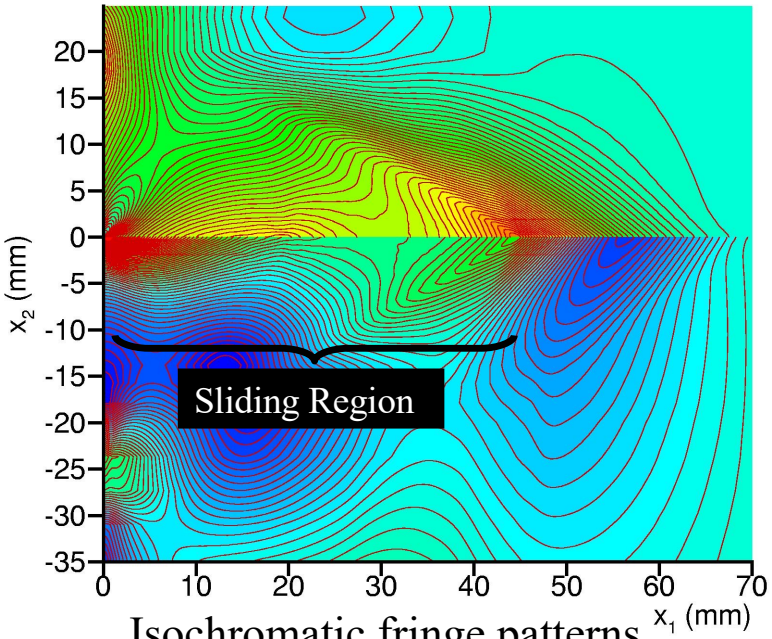

Isochromatic fringe patterns

$$\dot{T}_s = C_s(\Delta\dot{u}_s - \mathrm{sgn}(T_s)\Delta\dot{u}_{slip})$$

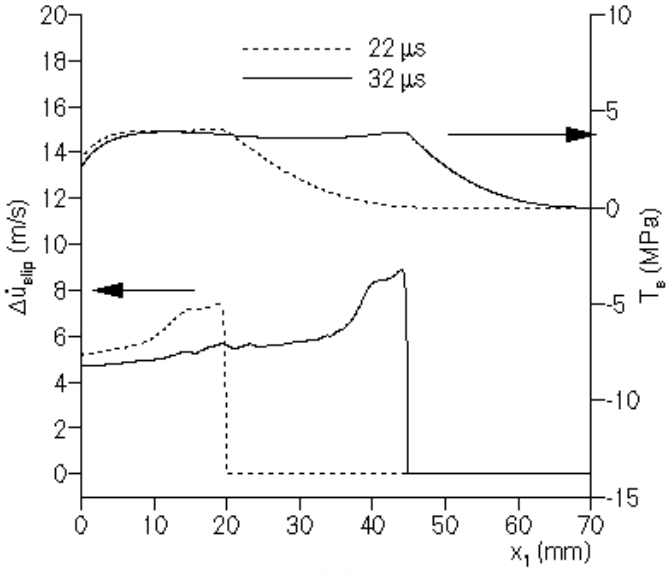

Sliding rate and shear traction

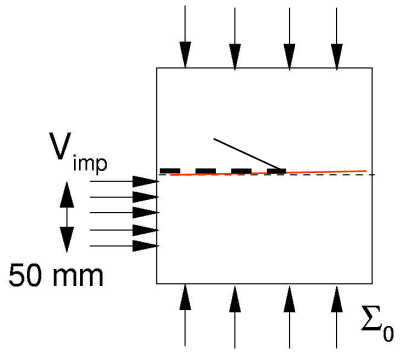

Case II: Results for Σ_o =30 MPa, V_{imp}=2 m/s

High compressive stress →
Self-healing slip-pulse

$$\dot{T}_s = C_s(\Delta\dot{u}_s - \mathrm{sgn}(T_s)\Delta\dot{u}_{slip})$$

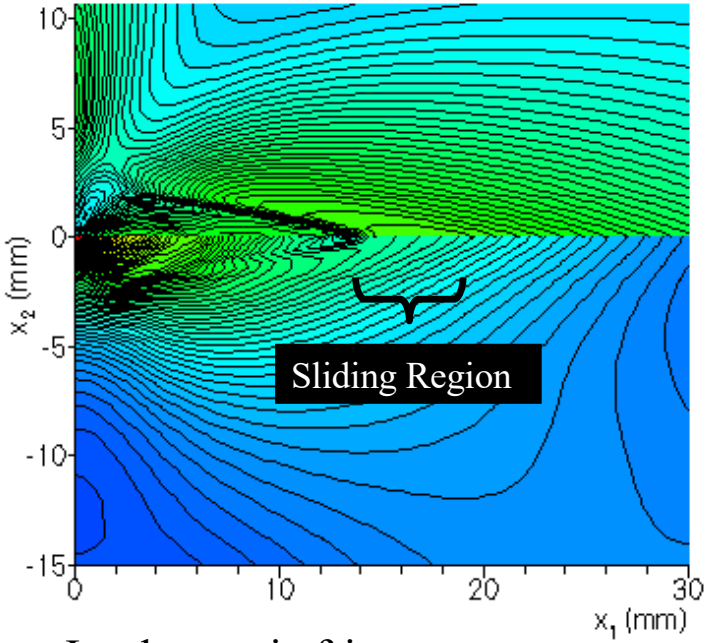

Isochromatic fringe patterns

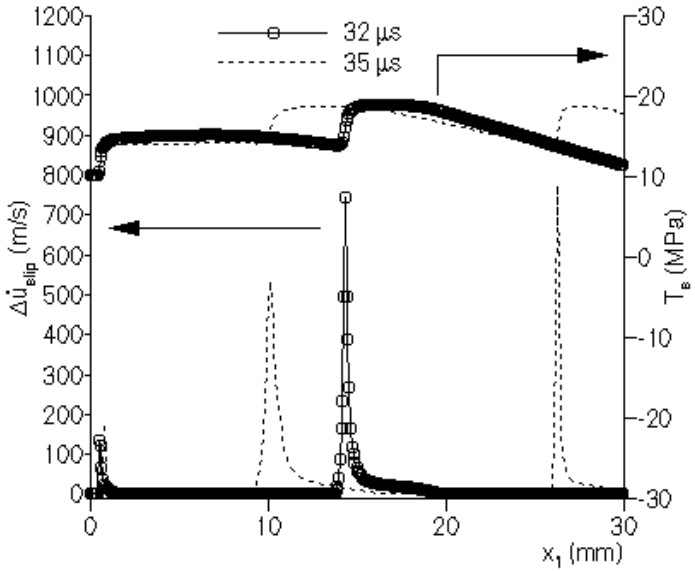

Sliding rate and shear traction

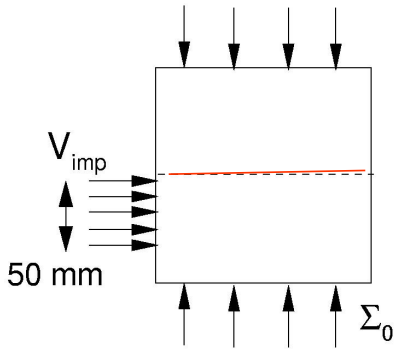

Case III: Σ_o =10 MPa, V_{imp}=20 m/s

Intermediate compressive stress and high impact speed → Quasi-periodic slip-pulses

$$\dot{T}_s = C_s(\Delta\dot{u}_s - \mathrm{sgn}(T_s)\Delta\dot{u}_{slip})$$

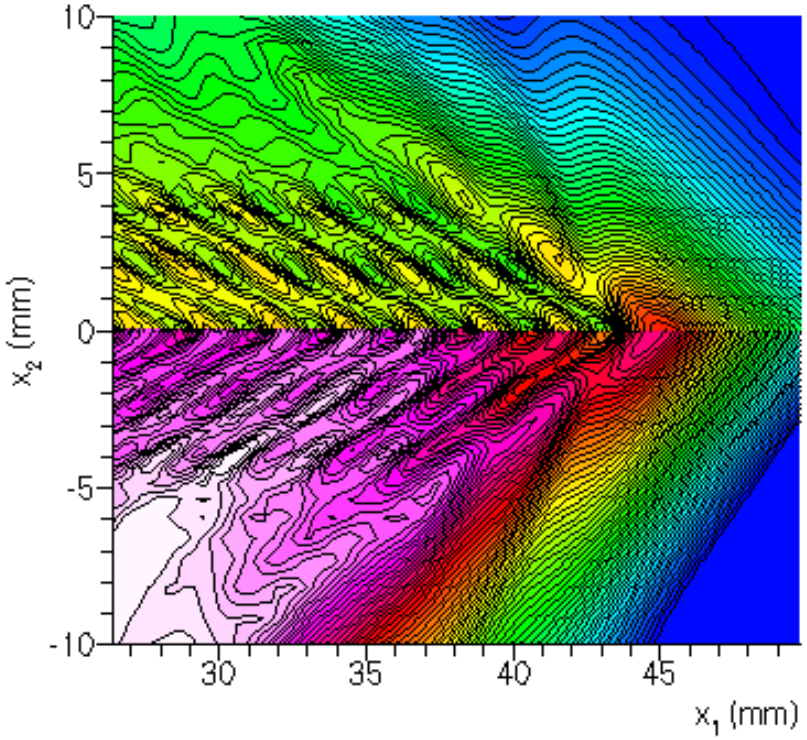

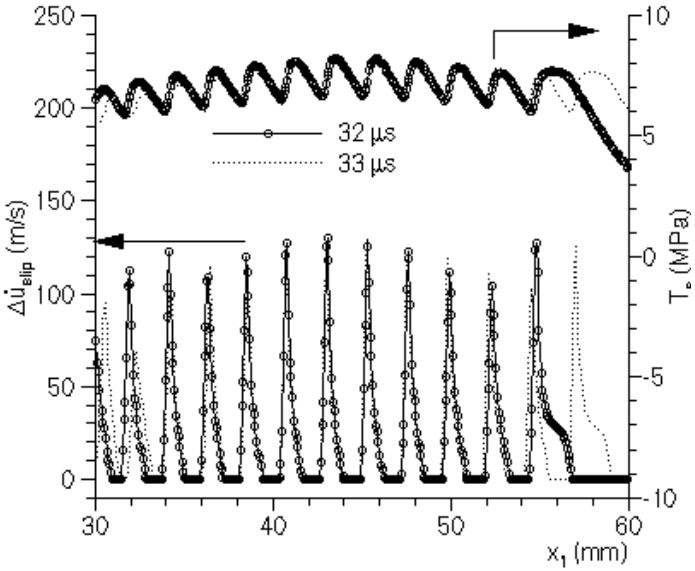

Transient slip pulses observed in experiments :

Propagation speeds $\sqrt{2}\, c_s < v < c_l$ with associated shear Mach waves

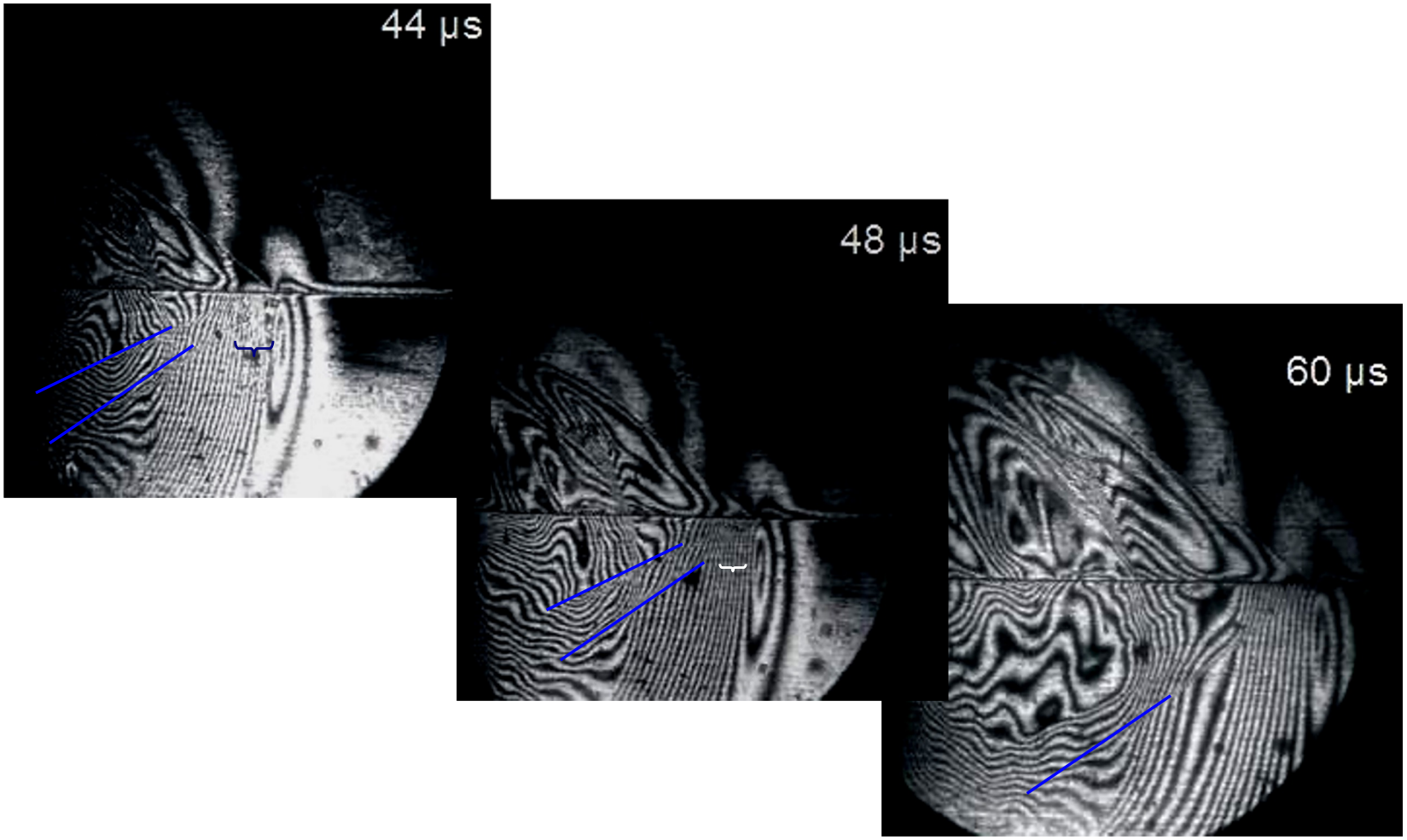

Evolution of frictional sliding from multiple pulses to crack-like sliding region

Σ_o =0.9 MPa V=10 m/s

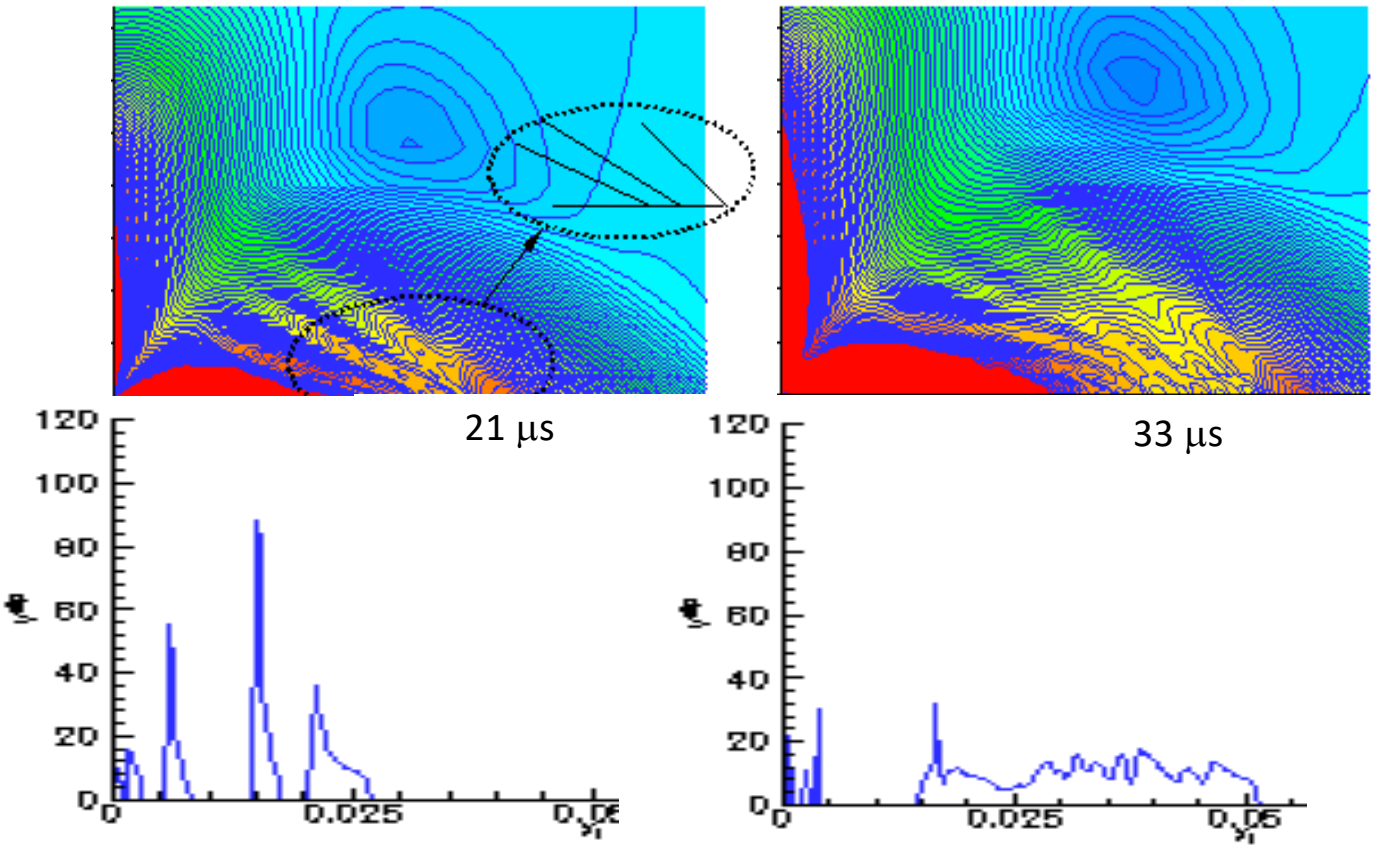

Frictional sliding tip propagation speed

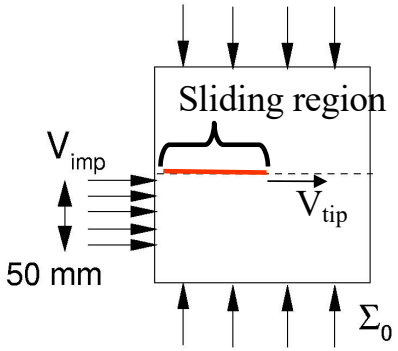

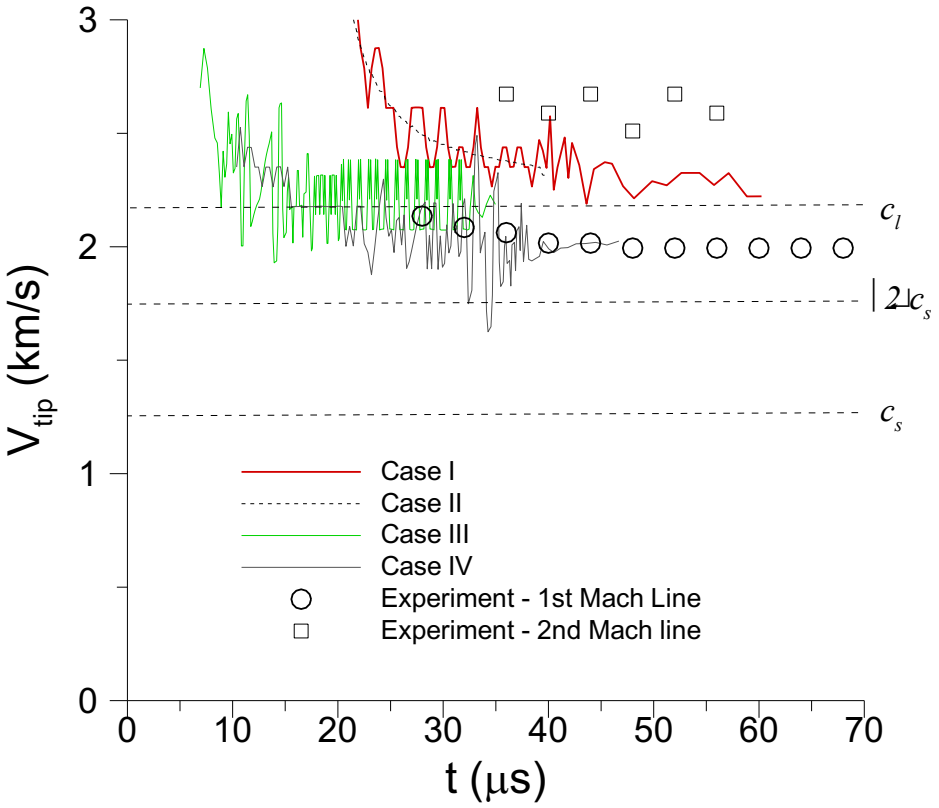

The frictional sliding mode depends on the compressive stress and the impact velocity

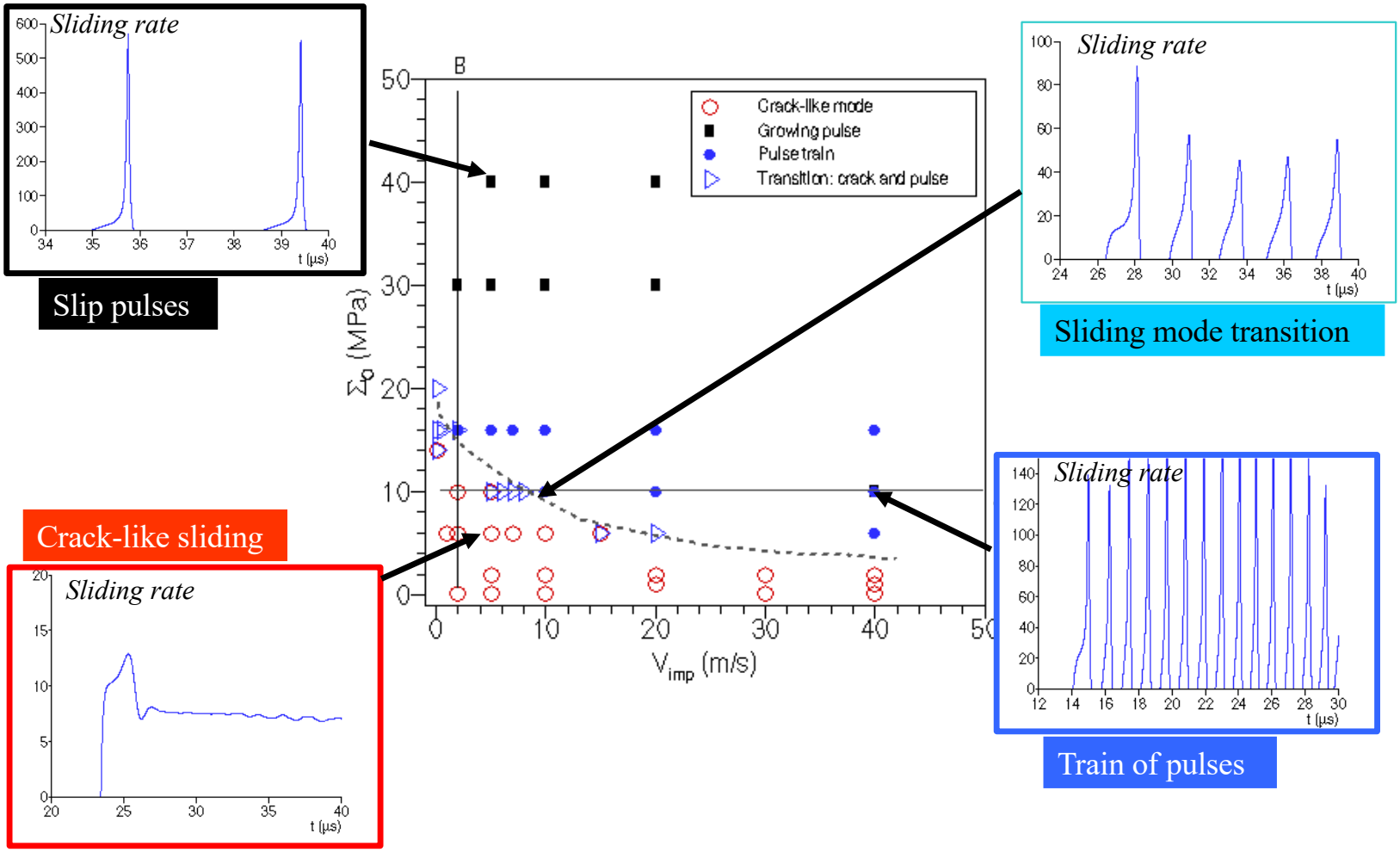

Total frictional sliding and total displacement jump across the interface

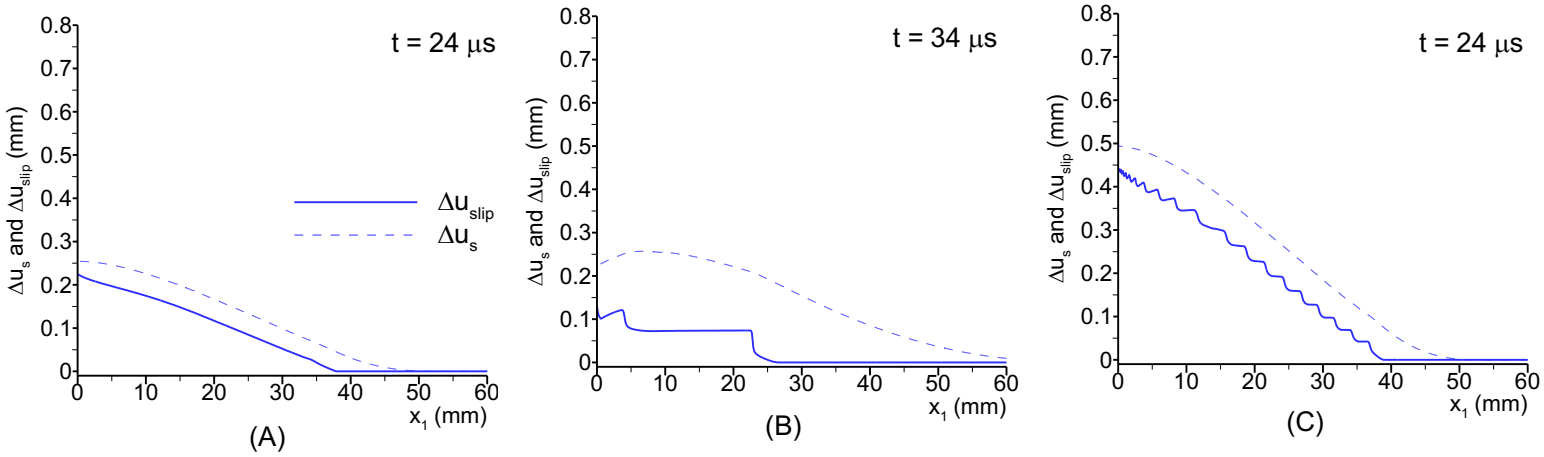

Case I:
Expanding crack-like frictional sliding

Case II:
Self healing slip-pulse

Case III:
Quasi-periodic slip-pulses

Pulse-like and crack-like ruptures in experiments

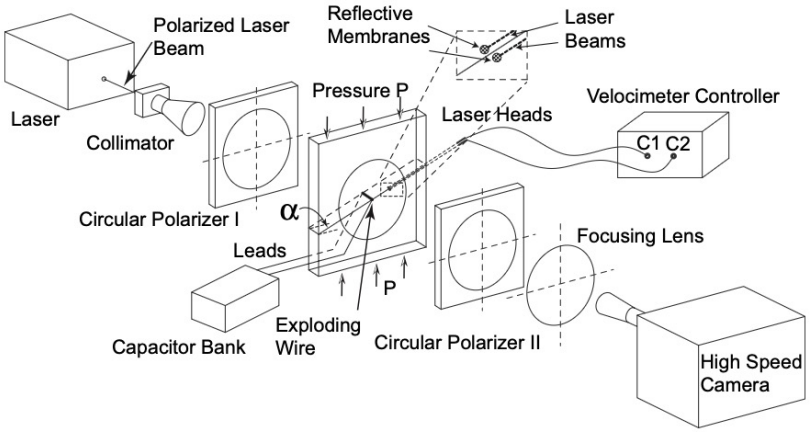

Fig. 1. Specimen configuration and experimental setup. Far-field pressure *P* and the inclination angle α are system variables. Dynamic photoelasticity and high-speed photography were used along the optical axis. Two velocimeters measured fault-parallel particle velocity histories above and below the simulated fault. The capacitor bank and exploding wire configuration provided the rupture initiation mechanism and the synchronizing trigger.

Lu,Lapusta and Rosakis (*PNAS*, 2007)

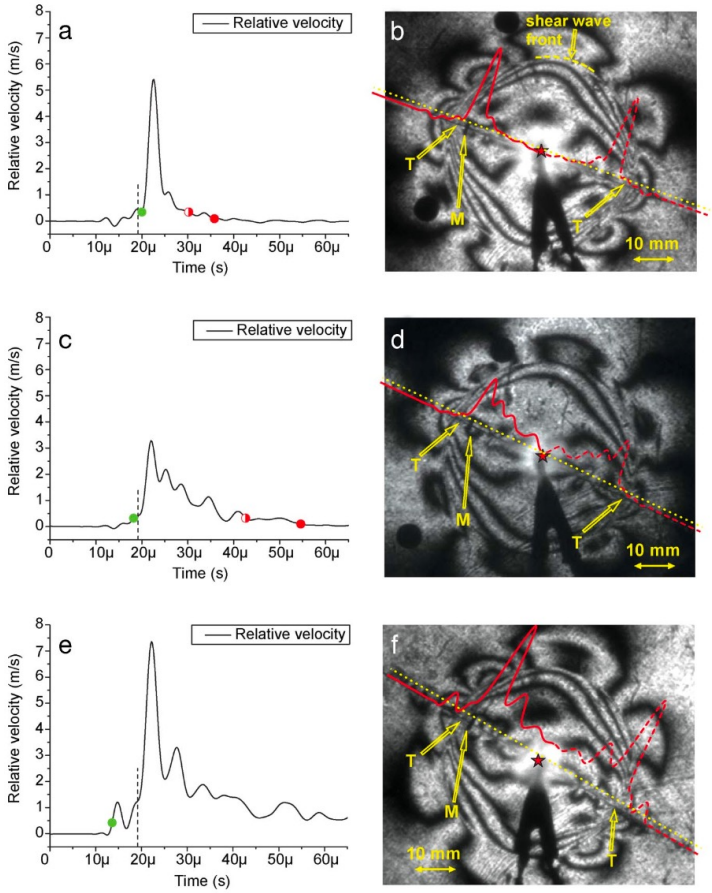

Fig. 2. Three representative rupture modes corresponding to different inclination angles. (*a* and *b*) A narrow sub-Rayleigh pulse for $\alpha = 20°$. (*c* and *d*) A wider (*e* and *f*) A sub-Rayleigh pulse for $\alpha = 25°$.(*e* and *f*) A sub-Rayleigh crack-like rupture for $\alpha = 30°$. Compression load *P* is 10 MPa for all three cases. (*Left*) Relative velocity histories recorded at 20 mm distance from the hypocenter. The dashed lines indicate the time of the shear wave arrival. The green fully filled dots indicate the estimated initiation time of interface sliding. The red half-filled and fully filled dots indicate two estimates of interface locking time. Note that there are no estimates of locking time marked in panel e because the interface in that case experiences no locking at the measurement location within the window of observation. (*Right*) Contours of maximum shear stress captured at 22 μs after rupture initiation. Letters T indicate rupture tips. Letters M indicates the measurement location for the two velocimeters. The relative velocity record is superimposed on the photoelastic pattern to facilitate the analysis of rupture behavior. The yellow dotted lines indicate the value of the elastic cut-off velocity for each case.

Dynamic friction simulations using Rate-State Friction Law

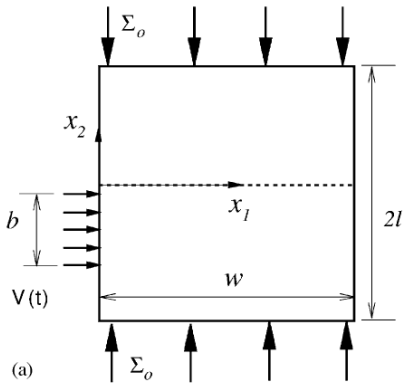

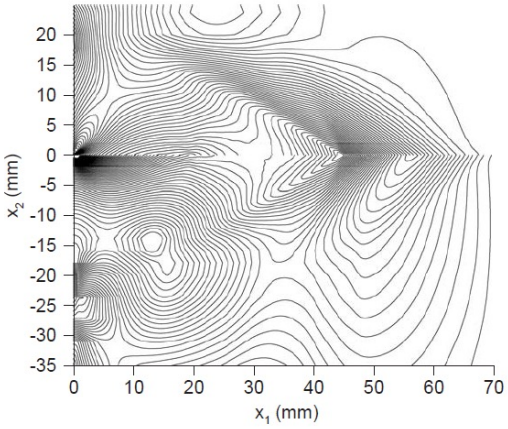

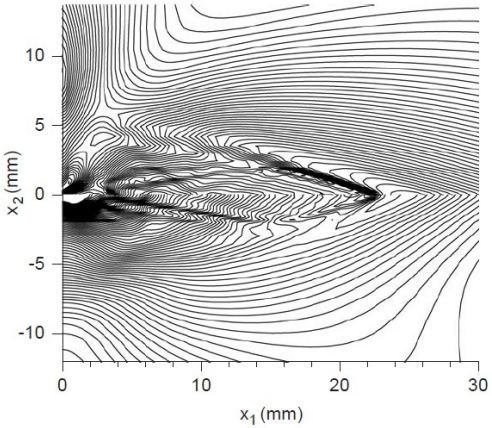

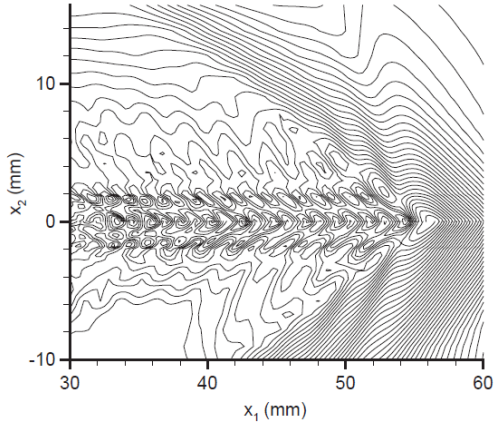

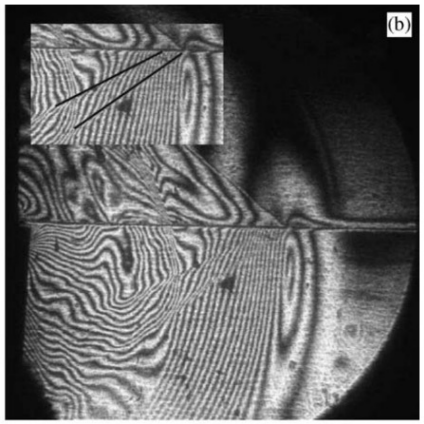

Crack-like

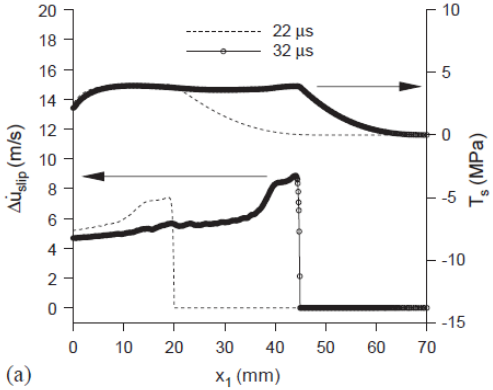

Pulse-like

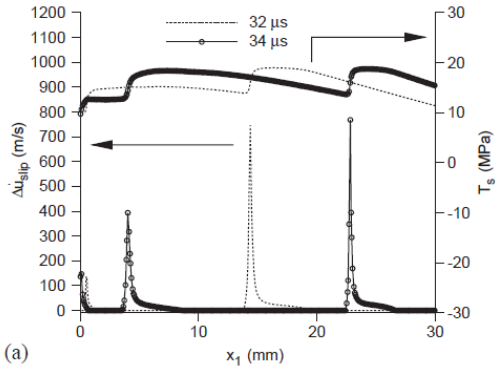

Train of pulses

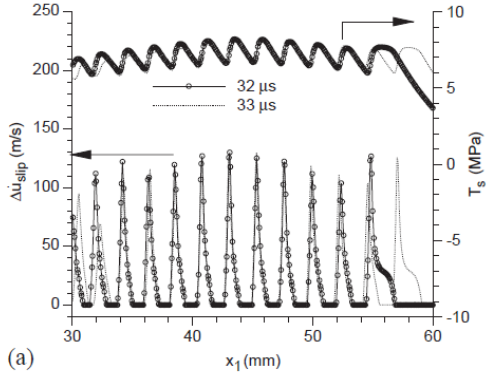

Coker, Lykotrafitis, Rosakis, Needleman (*JMPS*, 2005)

Dynamic friction simulations using Rate-State Friction Law

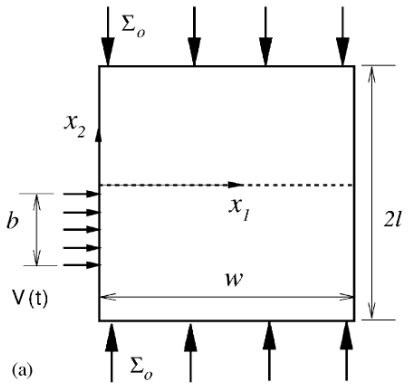

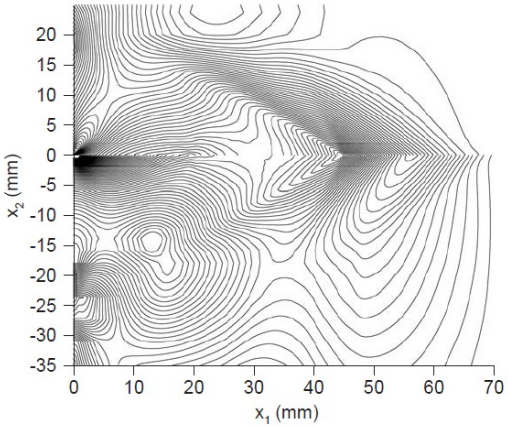

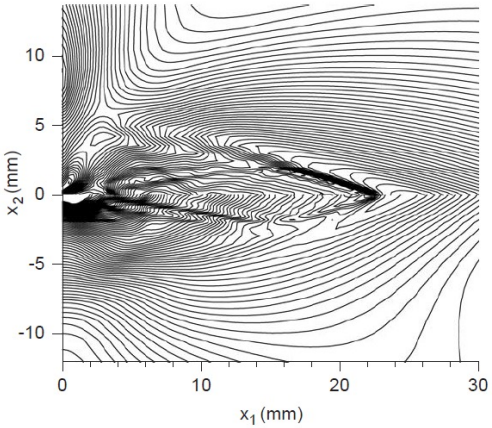

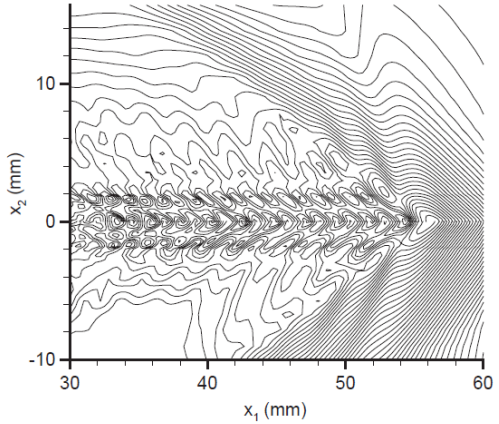

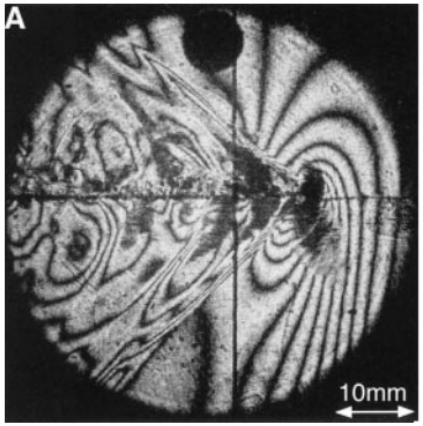

Crack-like

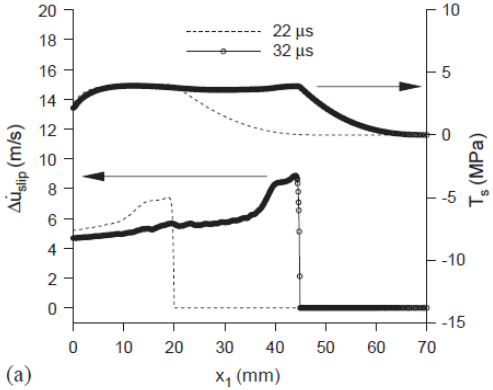

Pulse-like

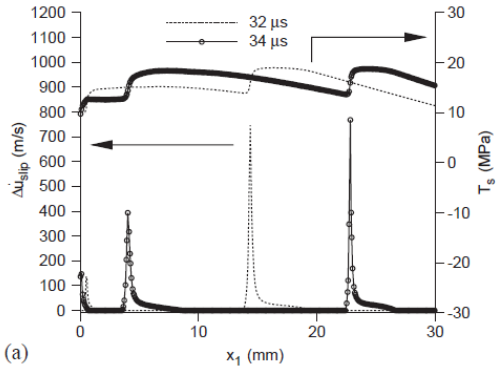

Train of pulses

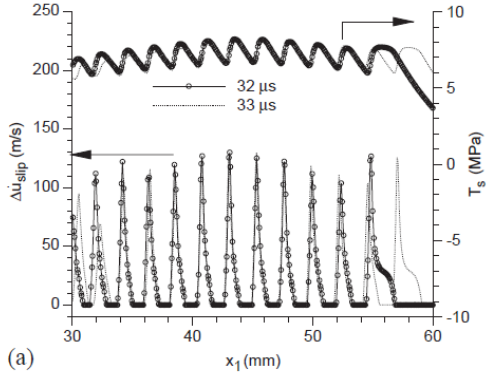

Rosakis, Samudrala, Coker (*Science*, 1999)

Friction to Fracture

Svetlizky, Bayart and Fineberg (*Annu. Rev. Condens. Matter Phys.*,2019)

- Traditional view: an interface remains stationary until shear stress reaches a threshold (static friction μs), then slides uniformly.
- Modern view: frictional slip initiates via propagating rupture fronts — not by simultaneous failure of the entire interface.
- Svetlizky, Bayart & Fineberg: frictional rupture fronts generate singular stress fields consistent with Linear Elastic Fracture Mechanics (LEFM).
- Macroscopic motion emerges only after a rupture front traverses the entire interface.

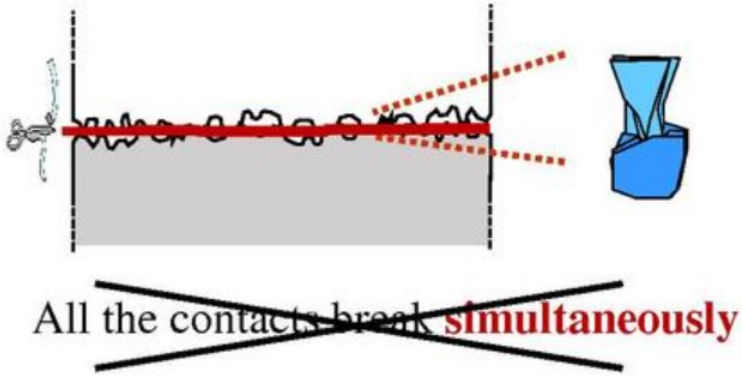

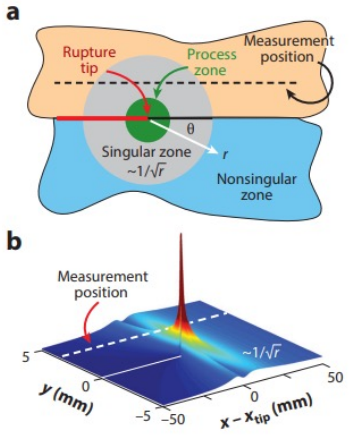

Why Brittle Fracture Theory for Friction?

Frictional onset = rupture

LEFM replaces static friction laws

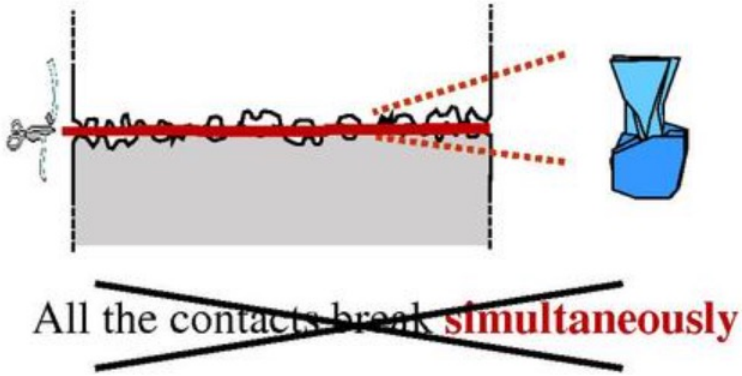

- Frictional slip initiates via rupture fronts, not static thresholds.
- Rupture fronts behave like dynamic shear cracks.
- This view unifies friction and fracture theory.

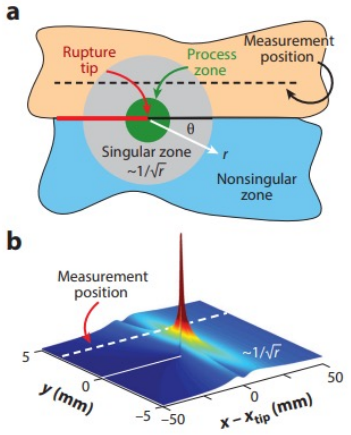

"Things don't break all at once — friction initiates as a propagating crack."

Svetlizky, Bayart and Fineberg (*Annu. Rev. Condens. Matter Phys.*,2019)

LEFM Description of Frictional Rupture

- Near the rupture tip, the stress field has a singular form:

$$\sigma_{ij}(r,\theta) = \frac{K_{II}}{\sqrt{2\pi r}} f_{ij}(\theta, C_f)$$

where K_{ii} is the mode-II stress intensity factor; Cf is the rupture front velocity

- The energy release rate $G = K_{ii}^2/E$, governs whether the rupture propagates: G = Γ at the tip.
- Fracture energy Γ, not the friction coefficient, is the fundamental parameter controlling rupture onset.
- Γ is proportional to the real contact area A — higher A means more energy needed to break the interface.
- This framework predicts rupture speed, arrest conditions, and stress radiation quantitatively.

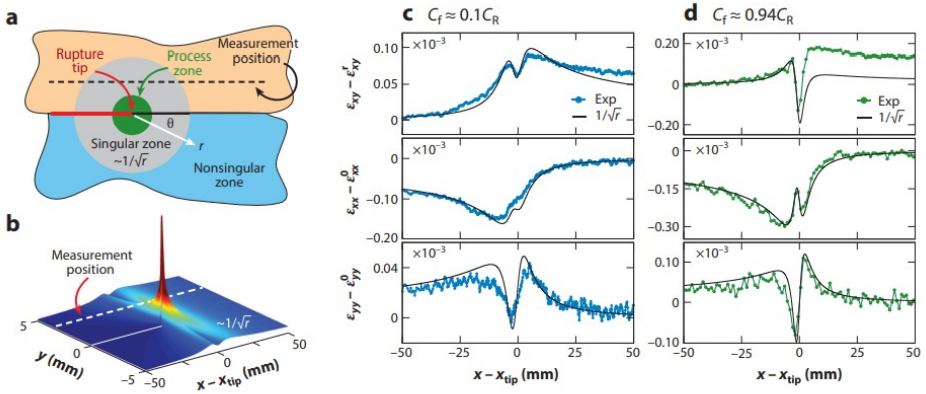

Figure 2

The $1/\sqrt{r}$ form of the elastic strains. (*a*) Stresses at the vicinity of the crack tip have a universal $1/\sqrt{r}$ singular form (*gray region*). Singular stresses are regularized in the process zone (*green region*), where dissipation takes place. Nonsingular contributions should be taken into account at distances from the crack tip where they become comparable with the singular contribution. (*b*) The calculated shear strain ε_{xy} surrounding the rupture tip predicted by Equation 5 for $C_f = 0.1C_R$. The white dashed line corresponds to the strain measurement location relative to the frictional interface $y = 0$. Note the angular dependence that drives the rapid oscillations evident in the measurements presented in panels *c* and *d*. Measurements of strain tensor variations, ε_{ij}, slightly above the frictional interface ($y = 4$ mm), for (*c*) a slowly propagating rupture ($C_f \approx 0.1C_R$) and (*d*) a rapid rupture ($C_f \approx 0.94C_R$). These measurements were acquired during the rupture events presented in **Figure 1*d*,*e***. The corresponding LEFM predictions of Equation 5 are plotted in black. Here, both measurements were performed for the same normal load but for different values of the imposed shear. In both, $\Gamma \approx 2.5$ J/m^2 is the sole free parameter. ε^r_{xy}, ε^0_{xx}, and ε^0_{yy} are, respectively, the residual shear strain after passage of the fronts and the initial values of the strain tensor in the propagation and normal directions. Data taken from Reference 86. Abbreviation: LEFM, linear elastic fracture mechanics.

Svetlizky, Bayart and Fineberg (*Annu. Rev. Condens. Matter Phys.*,2019)

➡ Γ is proportional to A

➡ **A** is proportional to σ_{yy}

(Bowden and Tabor picture)

➡ Γ is proportional to σ_{yy} !

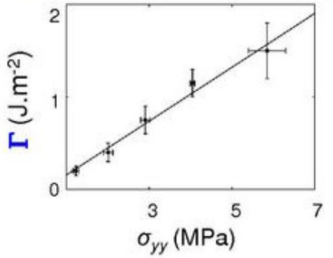

THANK YOU

Acknowledgements:

RÜZGEM (METU Center for Wind Energy Research)